Flexible Floating Island

Yun Liu

Master of Science Thesis

TU Delft Delft University of Technology

Flexible floating island

Master of Science Thesis

by

Yun Liu

To obtain the degree of Master of Science
at the Delft University of technology

Student number: 4435370

Thesis committee:

Prof. dr. A.Metrikine,	TU Delft - Chairman
Ir. C.Keijdener,	TU Delft - University supervisor
Dr.ir. F. Pisanó,	TU Delft - University supervisor

April 12, 2019

Faculty of Mechanical, Maritime and Materials Engineering
Delft University of Technology

TU Delft Delft University of Technology

Abstract

Nowadays, fears over rising sea levels due to global warming have prompted many countries with lands below sea level to find solutions to ensure the safety of nation and citizen. Furthermore, the development and utilization of marine resources have always been a topic of interest. Due to these necessities, the concept of flexible floating islands that can be used for fish farm, energy islands and residence has emerged. The flexible floating island consists of many smaller identical triangles connected by springs. This design is convenient for installation, disassembly, and diversification of functions.

The main objective of this thesis is to investigate and analyze the forces acting on and motions of the flexible floating islands due to the interaction with regular waves; a numerical model is an excellent way to complete that mission.

The floating islands in waves that are constrained with mooring lines have translational and rotational motions under the combined effect of hydrodynamic, hydrostatic, gravitational and mooring forces. The approach for solving the forces starts with linear potential theory, which means that uncompressed inviscid flow is assumed. After marking out the identical smaller panels on the wetted surfaces of each small triangle, the interface conditions between the triangle and the fluid are satisfied, thereby obtaining the source strength for each panel. With the expressions for the potentials, all the hydrodynamic coefficients including added mass, damping and wave exciting forces can be evaluated.

Finally, the response of islands can be evaluated by using the equations of motions of the island in the time domain and converting them to the frequency domain. Two models are created in this thesis, a single island model and a two-island model, the former focuses on learning the methods for solving the hydromechanics coefficients, and the latter focuses on the hydrodynamic interaction between the two islands.

Acknowledgements

The successful completion of this thesis would not have been possible without the guidance and support of many people who offered expertise and encouragements throughout the process. I especially want to thank:

Professor Andrei Metrikine for your inspiring advice and patiently interpretation as my thesis committee chairman. You always guide me in a professional and accessible way. You used many interesting and straightforward examples to inspire me when I got confused. Also, thank you for the amount of time for the meetings that you made available for me.

Chris Keijdener for your continues guidance and encouragements as my university supervisor. You are always quick to give advice and instructions on my problems even you have many other daily tasks. Thanks a lot for your encouragements in the most confused times of my thesis.

All my friends for your concern and support. Special thanks to Rui Zhu, Yaxi Peng, Pengpeng Xu, Wang Xi, and Hong Tan, for your constant care and help over the years. I am sure we will have a chance to have a good drink next time.

Last but certainly not least, to the unsung heroes of this thesis. Thank you to my parents for helping me come to the Netherlands and your unwavering belief in my ability to tackle the challenges.

Contents

Chapter 1

Introduction

1.1 Background

Due to human's over-exploitation and improper use of the environment, global warming is becoming a more severe problem. The sea level is rising and many countries with a land area below sea level like Maldives, the Netherlands and Belgium are trying to find solutions to ensure the safety of nation and people. On the one hand, some protections to prevent seawater intrusion have been built. On the other side, floating islands that are now being built around the world can solve this problem.

The history of the floating island can be traced back to prehistoric times; the ancient Celtic built their lake home ‘crannog' in Scotland and Ireland. Also, in south-east Asia, the fishermen in Cambodia have been living on water for centuries. They live entirely in floating villages on the Great Lake. Those floating villages changed heights and locations with water level variations (Koekoek, 2010).

From the 1960s on, multiple utopian ideas for floating cities arose. The futuristic-looking Lilypad floating city concept is one of the most well-developed ideas for a functioning sea community. Envisioned as a floating 'ecopolis' for climate change refugees, Vincent Callebaut's (2014) design resembles a water lily and would not only be able to produce its energy through solar, wind, tidal and biomass but would also process CO_2 in the atmosphere and absorb it into its titanium dioxide skin. Each of these floating cities could hold as many as 50,000 people.

Figure 1.1: A concept image of Lilypad floating city by Vincent Callebaut

As worldwide energy consumption increases and fossil fuels decrease, many types of energy become more and more precious. However, several durable forms of energy can be gained at sea, like wind, algae, thermal and wave energy. At the moment the technology of generating power out of waves is still in his infancy, but the technology looks promising. The availability of wave energy grows progressively as one harvest further offshore, so ocean colonization and developments in floating technologies play a crucial role in future events in wave energy conversion. Moreover, Floating agriculture is also an ideal way to relieve land and food stress. An additional advantage of floating agriculture could be that the ‘float lands' can be moved during the season, so the floating agriculture can always have an ideal climate. Besides, large super-large floating structure is the development and use of marine resources, necessary equipment, to meet the effective use of maritime space and the establishment of military bases in the sea and other needs.

Figure 1.2: Floating fish farm

Figure 1.3: Energy Island

1.2 Large floating structures

Large floating structures refers to the artificial islands, which can be used for floating airports, bridges, piers, fish farms, energy plants, and human's accommodations. Currently, several existing large floating structures have been built in many sea areas for a variety of different purposes; meanwhile, there are many floating structures under construction as well.

Compared with the permanent offshore structures which might extend from the shore into open water, floating structures has many advantages:

- The floating structures are easy to install and remove, they can be carried onshore for loading and unloading, and then towed to sea for operations;
- Most of the structural components can be recycled for reuse;
- The floating structures meet the environmental requirements, which will not cause harm to the local marine ecosystem;
- The floating structures do not cause silt deposition in deep harbors;
- The floating structures do not disrupt the ocean currents;
- The floating structures are immune to seismic shock.

The most significant difference between large floating structures and watercraft is the usable area, for the large floating structures, the effective useable space is the top surface. Thus a useful floating structure can be connected by joining the necessary number of floating units together. The design of the floating structure must comport with safety and strength requirements and operating conditions to ensure the safety of people and facilities on the structure.

As the references for this thesis, the Floating Piers, also named walkways, in Italy and Floating Cycle Path on the River Thames in England have similar principles as this project. The walkway is already under construction, will comprise 200,000 high-density polyethylene cubes that slot together in a modular manner. Visitors will be able to walk from Sulzano to Monte Isola and the island of San Paolo, or will be able to get a view of the installation as a whole from up in the surrounding mountains. As another example, the Floating Cycle Path will be used for sharing road space with fast-moving cars and vans to relieve traffic pressure and improve travel quality.

(a) Floating Piers (b) Floating Cycle Path

Figure 1.4: Large floating structures

1.3 Advantages, risks and precautionary measures of floating islands

1.3.1 Advantages

As previously mentioned, the floating island can be used as many functions. Compared with the traditional construction way for artificial islands, flexible floating islands have more advantages:

- **Environmental concerns**

As one's known, most existing artificial islands are made by reclamation, which may lead to a series of potential problems, such as the influence on coastal erosion, changes to area wildlife, the transport for alongshore sediment, the alter for wave pattern and weak soil due to constant exposure to rising sea water. In a word, a fixed island made from reclaimed land may lead to a significant impact on the surrounding environment. Several improvements of floating islands can ameliorate this concern. The floating structures do not cause silt deposition in deep harbors, do not disrupt the ocean currents and they are immune to seismic shock.

- **Reconstruction and recycling**

The expansion and renovation are very hard for fixed reclamation islands. Its construction period is far-off, and construction must be carried out offshore, which means some maritime activates may reduce or even stop due to the construction. Moreover, if the island deeply destroyed the local environment, its demolition work also requires a lot of money and time. In contrast, floating islands can be installed onshore and then carried to offshore by tow. This feature decides it can be recycled readily as well. In this project, the large floating island consists of multiple small triangle islands. If a problem does occur in one of the islands, replacement or maintenance is very convenient.

- **Sinking islands**

The floating islands do not like the fixed reclaimed islands that are confronting the sinking problem due to seawater scour, corrosion and sediment loss, which ensures the safety for the people and assets on the islands.

1.3.2 Risks

Regarding the constructed artificial island and related materials, some potential risks must be considered.

The first one is the wave height, the height of floating structures and corresponding countermeasures should be considered under the condition of extreme wave height in the local sea area. Then is the impact on the surrounding marine environment, there is no doubt that a new offshore structure will more or less in influence the original balance of the local ecosystem including marine life and climate. The third one is the expenses and benefits. This economic problem is related to the budget for the construction of artificial islands. Additionally, pollutions are also serious problems. The waste during construction and living garbage should be handled properly to avoid contaminating the local environment

1.3.3 Precautionary measures

To prevent the above risks, some precautionary measures are essential. For the wave height, on the one hand, based on the statistics of wave data and obtain an accurate prediction for the extreme wave height is indispensable. On another hand, some externally enhanced measures like wave blockers can absorb part of the wave energy and reduce the wave force that acts on the floating islands.

For the environmental problems, that the floating islands leave enough space to not disturb the life of the sea creatures, on that basis, island siting and scale is also an essential preparatory work.

The expenses and benefits are mainly referred to the budget, the scale and functions of the island depend on its investment. The financial problem will not be discussed in this paper in details; it can be regarded as a further recommendation.

The pollution can be divided into two parts: construction waste produced in the construction process and living waste produced in the daily work process. For the former one, the manufacturing and welding work can be done onshore, and then transport to sea for assembly. For the latter one, some garbage disposal points will be set up on islands to collect domestic production of garbage regularly. Besides, a small sewage treatment system on the island will be used to treat wastewater.

1.4 Focus of the research

To investigate and analyze the hydrodynamic forces and motions of flexible floating islands, a numerical model is an excellent way to complete that mission. The focus of this research is the behavior of islands under the effect of waves. Waves will flock to the island from all directions, and each part of the island will have the translations (surge, sway and heave) and rotations (roll, pitch, and yaw). In particular, one part's behavior is also influenced by the others due to springs connect them. More details will be discussed in chapter 2 and 3.

1.5 Approach

In this thesis, the motions of islands will be analyzed numerically. In the new numerical model, the movements and loads of islands are analyzed. The equations of motion are entered to the programming to address the motions along the time and the frequency. The hydrodynamic characteristics need to be solved by way of describing hydrodynamic coefficients of the single island model and the multiple islands model. In this process, the parameters of islands are designed based on the environmental conditions and its functions. Next, a numerical model is required to

simulate the forces that implemented on the islands, which may include hydrostatic force, hydrodynamic force, gravity, etc. During the analysis, an uncompressed inviscid flow is being assumed, which is described in details in chapter 2. Finally, through the model, the motions in different modes of two models are expected to be predicted for achieving the target of building the flexible floating islands

In conclusion, the single island model and the two islands model will be built separately and concentrating on the research of their responses in waves in this thesis.

Chapter 2

Single island model

In this chapter, a single island is being analyzed. The motion of the island is based on an essential assumption that the wave excitation loads and islands motion responses are assumed to be linear. Also, we assume that the transmitted wave is a harmonic and regular wave. The focus is the hydrodynamic effect on a floating structure, and the analysis is mainly on the basis of the potential theory and the Lagrangian formalism. The goal of this chapter is to research the motions of the floating island under the effect of waves based on the given data to ensure the working conditions do not exceed the limiting conditions. Besides, the multibody case to investigate the connecting method and coupling effect will be discussed in the next chapter that on the basis of this chapter.

2.1 The design of the island

2.1.1 Dimension parameters

There is a great diversity of shapes of the island as options. An equilateral triangle is a selection in this case on account of its common and easily constructed form, and it can be easily disconnected and interchanged. Assuredly, other shapes can also be used, and the triangle is just a reasonably characteristic shape.

One pivotal thing should be noticed before designing the parameters of the island is to determine the coordinate system. In this case, the floating island has six degrees of freedom. Hence, three coordinates are needed to determine the motions for translations: surge, sway and heave, and another three coordinates to determine the motions for orientations: roll, pitch, and yaw.

In this project, the origin is settled at a fixed point that is on the mean water surface in terms of researching the response of island in waves due to it is a clear and straightforward technique to record the variation of motions of the island in a time series and one can observe the offset from the initial position readily. Thus, the center of gravity is located at $(0,0,z_c)$ in this case. The single island coordinates defined in the earth-fixed coordinate frame can be denoted by:

$$x_i = [x \quad y \quad z \quad \phi \quad \theta \quad \psi]^T \tag{2.1}$$

In which, x, y, z represent surge, sway and heave displacement respectively, i denotes the mode. Similarly, ϕ, θ and ψ represent roll, pitch, and yaw angle respectively.

It is clear to see that the floating island has a lateral symmetry in shape and weight distribution. Thus surge-heave-pitch will be decoupled from sway-roll-yaw (Das and Das, 2004).

The main parameters of the triangle, which include the length, width, height and wall thickness are depending on its function, cost, transportation, materials, and local environment. Of foremost, all designs for the offshore structures are inseparable from the environment, especially the water depth. For this case, the floating island will be built in the North Sea. The location of the floating island is generally chosen to be close to the coast, so the mean sea level of the selected area is 80 meters, and the wave height is 2 meters. Some wave parameters are shown in table 2.1.

Table 2.1 Wave parameters

Wave type	Wave height (m)	Wave amplitude (m)	Wave frequency range (rad/s)	Water depth (m)
Monochromatic wave	2	1	0~2	80

Based on the existing data and considering the scale of this project, the floating island is designed as an equilateral triangle that has a width of 60 meters and height of 6 meters; the wall thickness is 0.2 meters everywhere. All the parameters mentioned above are described in figure 2.1 and table 2.2. The coordinate system x,y,z is also shown in figure 2.1. The origin is on the mean water surface, aligning with the center of gravity of the triangle.

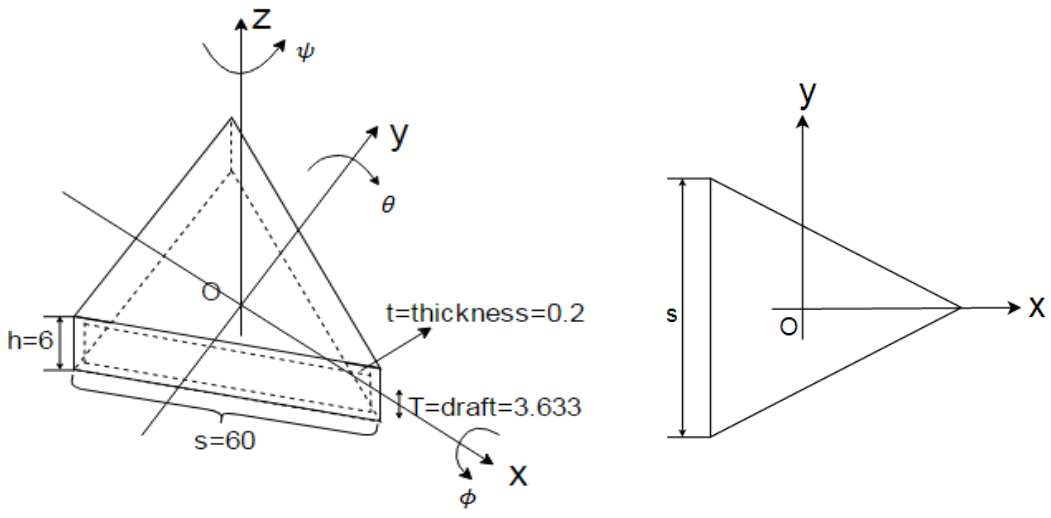

(a) Stereoscopic view of the floating island (b) Top view of the floating island

Figure 2.1: The single floating island

Table 2.2 The dimensions of triangle island

side length(m)	side height	wall thickness (m)	steel density (kg/m^3)	draft(m)	mass (kg)
60	6	0.2	7850	3.633	5805421

2.1.2 Mooring configuration

Mooring is a system in which a floating structure is secured to forestall free movement of the body on the water that keeps the offshore floater on its location during the design life.

Generally, the mooring lines can be considered as linear or non-linear depending on the material and complexity of the mooring system. In this thesis, the mooring lines are thought to be linear springs. To study its rationality, one characteristic of mooring lines that need to be determined is whether the linear theory applies to the relationship of tension and elongation. Depending on the research of the mooring lines in different materials by Riaan (2017) that shows in figure 2.2, the line tension-elongation curve shows a linear relationship within a certain elongation range when the chains and wires are made of steel, however, another curves shows a non-linear variation when the mooring lines are made of polyester.

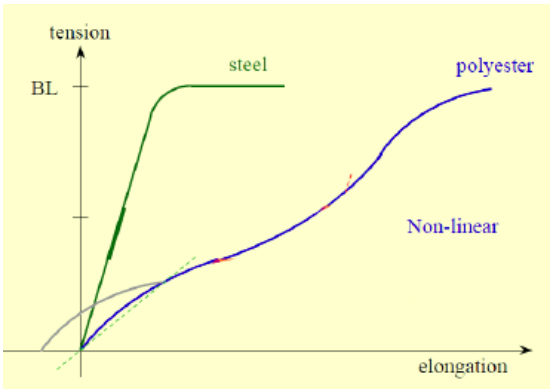

Figure 2.2: Tension-Elongation curves for different materials of mooring lines

Thus, an assumption in this project is the mooring lines are simulated as linear springs that stiffness always equal to the ratio of the load to the displacement that can be expressed as follows:

$$\vec{F}_{ext} = K_{mooring} \cdot \vec{x}_{island} \tag{2.2}$$

Where $\vec{F}_{ext}$ represents the external loads, $K_{mooring}$ represents the stiffness coefficient of mooring lines, and $\vec{x}_{island}$ represents the displacement of the floating island.

Three identical translational springs of stiffness k_0 are installed at the three

midpoints of corners of triangle separately to provide the normal restoring force in x-y plane. The other ends of spring are connected to three fixed points respectively. Besides, a rotational spring of stiffness k_r is set up at the center of the triangle to restrain the rotation of triangle in the x-y plane. This rotational spring is fastened to a monopile that does not affect the motions of the structure. This configuration can be comprehended more intuitively through figure 2.3.

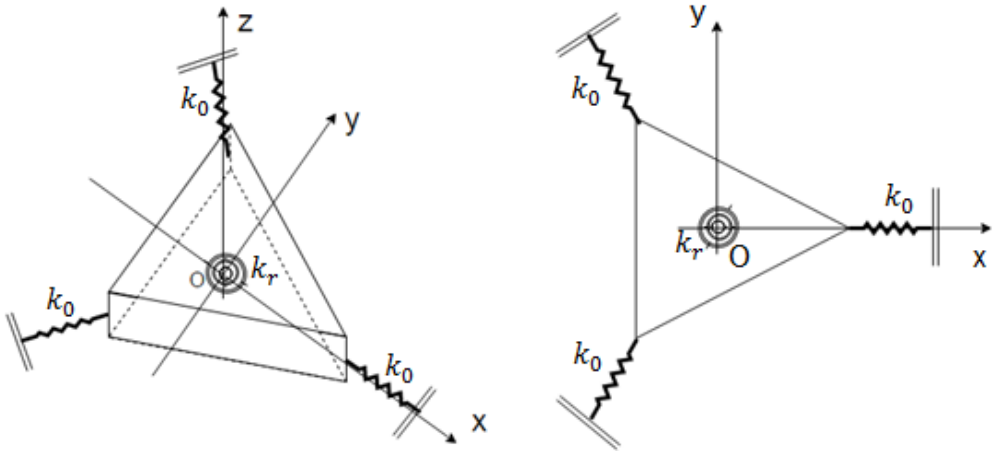

(a) Stereoscopic view (b) Top view

Figure 2.3: Mooring configuration for the single island

In this practical application, the floating flexible floating islands will be used for fish farm, energy island or human's offshore accommodation. These purposes determine that the floating island will not be too far away from the land, which means the mooring configuration above is convenient to implement. Furthermore, this configuration has many merits, such as simply manufacturing, easy disconnecting and an exquisite symmetrical outline. The values of stiffness coefficients k_0 and k_r are shown in table 2.3. The detailed determination method for k_0 and k_r is interpreted in section 2.3.6.

Table 2.3 The stiffness coefficients of mooring springs for the single island

Stiffness	k_0 (N/m)	k_r (Nm)
Values	$1.567 * 10^7$	$2.226 * 10^9$

2.2 Potential theory

Potential theory is one of the essential theories in this thesis. A description of the potential theory and the conditions that it has to be fulfilled will be discussed in this section. It should be noted that the fluid is treated as a continuous, homogenous, incompressible and irrational fluid. Namely, the shear force is nonexistence due to the inviscid flow. The density of fluid ρ is regarded as a constant in this thesis to guarantee the feasibility of potential theory.

2.2.1 Potential function

A velocity potential, Φ, is briefly a mathematical function that has the attribute that the velocity component in a spot in the fluid in any given direction equals to the derivative of this potential function in that spot to the given direction, which can be expressed as:

$$\dot{x} = \frac{\partial \Phi}{\partial x} \quad \dot{y} = \frac{\partial \Phi}{\partial y} \quad \dot{z} = \frac{\partial \Phi}{\partial z} \tag{2.3}$$

All potential theory solutions must satisfy the Laplace equation and rotation free condition (see Appendix A).

1. Laplace equation:

$$\frac{\partial^2 \Phi}{\partial x^2} + \frac{\partial^2 \Phi}{\partial y^2} + \frac{\partial^2 \Phi}{\partial z^2} = 0 \tag{2.4}$$

2. Rotation free:

$$\frac{\partial \dot{x}}{\partial y} - \frac{\partial \dot{y}}{\partial x} = 0 \quad \frac{\partial \dot{x}}{\partial z} - \frac{\partial \dot{z}}{\partial x} = 0 \quad \frac{\partial \dot{z}}{\partial y} - \frac{\partial \dot{y}}{\partial z} = 0 \tag{2.5}$$

2.2.2 Undisturbed wave potential

According to the linear potential theory, the velocity potential Φ of a floating structure is a superposition of the undisturbed wave potential Φ_0, diffraction wave potential Φ_7 and radiation potentials due to six structure's motion Φ_{rj}, note that $j = 1, \dots 6$ are associated with six motion modes of the floating structure.

$$\Phi = \sum_{j=1}^{6} \Phi_{rj} + \Phi_0 + \Phi_7 \tag{2.6}$$

Among them, the undisturbed wave potential is the easiest one to be obtained with a mathematical expression. First of all, if the wave moves in the positive x and y-direction and the angle with respect to the x-axis is μ, the form of the water surface can be expressed as a function of both x, y, μ and t as follows (Journee et al., 2008):

$$\zeta(x, y, t) = \zeta_a \cos(kx \cos\mu + ky \sin\mu - \omega t) \tag{2.7}$$

Then, the corresponding undisturbed wave potential for the regular wave with propagation direction μ in arbitrary water depth is:

$$\Phi_0 = \frac{\zeta_a g}{\omega} \frac{\cosh\big(k(d_0 + z)\big)}{\sinh(kd)} \sin(kx \cos\mu + ky \sin\mu - \omega t) \tag{2.8}$$

Where:

$\zeta_a = amplitude\ of\ \ undisturbed\ wave\ (m)$

$\omega = wave\ frequency\ (rad/s)$

$k = \dfrac{2\pi}{L} = wave\ number\ (rad/m)$

$L = wave\ length\ (m)$
$\mu = wave\ direction\ (rad)$
$d = water\ depth\ (m)$
$d_0 = distance\ from\ the\ origin\ to\ the\ seabed\ (m)$

2.3 Equations of motion

In this section, a structural model is designed for prediction of the movements and loading of the floating island. To this end, kinetic energy and potential energy deviate for the aimed object, and along with this, wave excitation forces are analyzed and formulated. Previous to this, simplification is the incoming wave is treated as a monochromatic wave, assuming linearity that means it is considered as a harmonic function with a certain frequency, a certain amplitude, and a certain phase angle to describe this regular wave in this thesis. One thing should be noticed before analysis is the meaning of the word 'linear' in this thesis represents four aspects: The first aspect is the linear description of the incoming waves that indicates linearized frees surface boundary conditions were applied when solving the Laplace equation. The second aspect is the linear approximations of flow effects arising from the presence on the floating island. The third aspect is the linear approximations of wave related properties, for instance, the wave pressure. The last aspect is the linear approximations of forces arising from integrating wave related pressures.

2.3.1 Lagrange equation

The Lagrange equation is a fundamental equation for analyzing mechanics and can be used to describe the motion of a body. The function of the Lagrange equation is equal to Newton's second law in Newtonian mechanics. Also, it is widely used to analyze mechanical problems when the latter is not fitting.

The standard Lagrange function L is defined as:

$$L = T - V \tag{2.9}$$

Where T and V are the total kinetic and corresponding potential energies respectively. The total kinetic energy is given by (Ghassemi and Yari, 2011):

$$T = \frac{1}{2}\sum_{i,j=1}^{6} m_{ij}\,\dot{x}_i\dot{x}_j + \frac{1}{2}\sum_{ji,j=1}^{6} a_{ij}\,\dot{x}_i\dot{x}_j \tag{2.10}$$

Where x_i is a generalized coordinate, $\dot{x}_i$ is a generalized velocity that comes from the time derivatives of the generalized coordinates, in which dot on the top denotes the derivative with respect to time. m_{ij} represents the generalized mass matrix. a_{ij} represents the added mass, it is worth noting that a_{ij} denotes the inertia in i-direction due to the motion in j-direction. The generic Euler-Lagrange equation is then obtained by:

$$\frac{d}{dt}\left(\frac{\partial L}{\partial \dot{x}_i}\right) + \frac{\partial D}{\partial \dot{x}_i} - \frac{\partial L}{\partial x_i} = Q_i \tag{2.11}$$

Where D is the so-called Rayleigh dissipation function, which allows accounting for radiation damping present in the system, it can be written as follows:

$$D = \frac{1}{2}\sum_{i,j=1}^{6} b_{i,j}\,\dot{x}_i\dot{x}_j \tag{2.12}$$

Where b_{ij} denotes the damping force in i-direction due to the motion in j-direction. Q_i is a generalized force acting along the generalized coordinate x_i. Each part will be solved separately in the following sections.

2.3.2 The assumptions for the hydrodynamic analysis

In this project, one of the essential assumptions of the model is the bottom plane (the plane in x-z plane in figure 2.3) of the triangle is the only surface that is considered in the analysis of the motions. Based on the design of this floating island, it is clear to see the mean submerged surface of the bottom plane is much larger than that of other planes. Thus the forces and motions due to the hydrodynamic effect on the bottom plane are stronger than that on the other planes. To make sure the island will not float away; four mooring springs with reasonable stiffness are implemented on the island that was described in 2.1.2. In other words, heave, roll, and pitch are the only three degrees of freedom that are considered for the motion analysis in this thesis.

Another assumption is the z-coordinate of the bottom plane is set as zero in the process of calculation for the hydrodynamic forces due to the draft of the floating island is small, especially when compared with the water depth. In other words, the radiation forces and the wave exciting forces are assumed to be applied on the mean water surface.

2.3.3 Mass

Mass and added mass are the prerequisite values to resolve the kinetic energy. The generalized mass matrix is given by (Salvesen et al., 1970):

$$\boldsymbol{M} = \begin{bmatrix} m & 0 & 0 & 0 & mz_c & 0 \\ 0 & m & 0 & -mz_c & 0 & 0 \\ 0 & 0 & m & 0 & 0 & 0 \\ 0 & -mz_c & 0 & J_4 & 0 & -J_{46} \\ mz_c & 0 & 0 & 0 & J_5 & 0 \\ 0 & 0 & 0 & -J_{46} & 0 & J_6 \end{bmatrix} \tag{2.13}$$

Where m is the mass of the floating island, J_i is the moment of inertia in the jth mode, J_{ij} is the product of inertia. Based on the 3-DOFs assumption, the mass matrix, in this case, can be written as:

$$\boldsymbol{M} = \begin{bmatrix} m & 0 & 0 \\ 0 & J_4 & 0 \\ 0 & 0 & J_5 \end{bmatrix} \tag{2.14}$$

The moment of inertia can be calculated as (Myers, 1962):

$$J_4 = m{r_i}^2 = \iiint_V {r_{roll}}^2 dm = \frac{m}{24}(s^2 + 2h^2)$$

$$J_5 = \frac{m}{24}(s^2 + 2h^2)$$

$$J_6 = \frac{ms^2}{12} \tag{2.15}$$

Where:
$J_i = moment\ of\ inertia\ (kg \cdot m^2)$
$r_i = the\ radius\ of\ gyration\ (m)$
$m = mass\ of\ the\ triangle = 5805421\ (kg)$
$s = side\ length\ of\ the\ triangle = 60\ (m)$
$h = the\ height\ of\ the\ triangle = 6\ (m)$

2.3.4 Added mass and damping

Within linear potential theory, the hydrodynamic forces onto a floating structure in waves can be considered as two categories: wave excitation forces and radiation force. The radiation force is the force onto an oscillating structure in still water, which can be categorized into the inertial force that proportional to the accelerations and the damping force that proportional to the velocities.

Added mass indicates the inertia added to a floating system when it is accelerated or decelerated relative to a surrounding fluid (Wallis, 2011). To be more specific, when a structure accelerates in an ideal fluid, scilicet non-viscous fluid, it must promote the surrounding fluid to accelerate. The fluid quality point backlashes on the structure to form resistance, which is called the resistance of fluid inertia. Therefore, the structure not only has to overcome the inertia of the structure itself but also overcomes the inertial resistance of the fluid when it is accelerating. The magnitude of the inertial resistance of the fluid is proportional to the acceleration of the structure motion, and the direction is opposite to the direction of the structure acceleration. The ratio of the inertial resistance of the fluid and the acceleration is namely the added mass, which always fetches its positive value. As a universal and non-negligible issue, added mass is of the same order of magnitude as the mass of the structure itself in the water in that the density of water is large so that it has to be added in the system.

Damping is a function that causes the dissipation of structural energy to reduce the amplitude of the motion of structure gradually. There are three primary sources of damping for the floating structures: potential damping resulting from radiating waves

carry energy away from the structure; viscous damping resulting from the structure generates eddies that take energy away from the system (eddies later dissipated into heat) and friction on shackles or mooring lines. By the assumption of inviscid fluid and little friction on mooring lines, the radiation damping is the sole source of damping.

As previously mentioned, surge-heave-pitch will be decoupled from sway-roll-yaw by taking account of the floating island has a lateral symmetry in shape and weight distribution, which also follows that the added mass and damping coefficients are (Salvesen et al., 1970):

$$\boldsymbol{A} = \begin{bmatrix} a_{11} & 0 & a_{13} & 0 & a_{15} & 0 \\ 0 & a_{22} & 0 & a_{24} & 0 & a_{26} \\ a_{31} & 0 & a_{33} & 0 & a_{35} & 0 \\ 0 & a_{42} & 0 & a_{44} & 0 & a_{46} \\ a_{51} & 0 & a_{53} & 0 & a_{55} & 0 \\ 0 & a_{62} & 0 & a_{64} & 0 & a_{66} \end{bmatrix}$$

$$\boldsymbol{B} = \begin{bmatrix} b_{11} & 0 & b_{13} & 0 & b_{15} & 0 \\ 0 & b_{22} & 0 & b_{24} & 0 & b_{26} \\ b_{31} & 0 & b_{33} & 0 & b_{35} & 0 \\ 0 & b_{42} & 0 & b_{44} & 0 & b_{46} \\ b_{51} & 0 & b_{53} & 0 & b_{55} & 0 \\ 0 & b_{62} & 0 & b_{64} & 0 & b_{66} \end{bmatrix} \tag{2.16}$$

Due to the heave, roll and pitch potentials are the only three terms that are considered for the radiation force analysis, the added mass and damping coefficients, in this case, are defined as follows:

$$\boldsymbol{A} = \begin{bmatrix} a_{33} & 0 & a_{35} \\ 0 & a_{44} & 0 \\ a_{53} & 0 & a_{55} \end{bmatrix}$$

$$\boldsymbol{B} = \begin{bmatrix} b_{33} & 0 & b_{35} \\ 0 & b_{44} & 0 \\ b_{53} & 0 & b_{55} \end{bmatrix} \tag{2.17}$$

The added mass and damping coefficients, $\mathrm{a_{kj}}$ and $\mathrm{b_{kj}}$, can be expressed (Journée and Massie, 2008) as follows:

$$a_{kj} = -Re\left[\rho \iint_{S_0} \phi_j \cdot n_k \cdot dS_0\right]$$

$$b_{kj} = -Im\left[\rho\omega \iint_{S_0} \phi_j \cdot n_k \cdot dS_0\right] \tag{2.18}$$

Where ρ is the density of seawater, ϕ_j is the space-dependent term of velocity potential that was mentioned in equation 2.8, S_0 is the mean wetted surface of the bottom plane, and n_k indicates the body's normal vector pointing into the water, which is given by:

$$
\begin{aligned}
&\text{surge:} && n_1 = \cos(n, x) \\
&\text{sway:} && n_2 = \cos(n, y) \\
&\text{heave:} && n_3 = \cos(n, z) \\
&\text{roll:} && n_4 = \mathrm{y}n_3 - zn_2 \\
&\text{pitch:} && n_5 = \mathrm{z}n_1 - xn_3 \\
&\text{yaw:} && n_6 = \mathrm{x}n_2 - yn_1
\end{aligned} \tag{2.19}
$$

It should be noted that the subscripts 1,2,..6 are used here to indicate the mode of the motion and k_{ij} denotes the restoring force in i-direction due to the motion in j-direction. Also, the following symmetry relationships need to be supplemented to the formula 2.16 is:

$$
\begin{aligned}
a_{kj} &= a_{jk} \\
b_{kj} &= b_{jk}
\end{aligned} \tag{2.20}
$$

2.3.4.1 Boundary conditions for radiation potentials

The only unknown values in equation 2.18 are the radiation potentials of harmonic waves that have to satisfy the Laplace equation and boundary conditions in this case:

1. The boundary condition at sea bottom:

Since the seabed is watertight, one kinetic boundary condition is:

$$
\frac{\partial \Phi}{\partial \mathrm{n}} = 0 \quad \text{at } \mathrm{z} = -\mathrm{d} \tag{2.21}
$$

Where d is the water depth.

2. Boundary conditions at the free surface:

The surface equation $\mathrm{S}(\mathrm{x}, \mathrm{y}, \mathrm{z}, \mathrm{t})$ can be defined as equation 2.22 because the particle is on the surface when that equation equals to zero.

$$
\mathrm{S}(\mathrm{x}, \mathrm{y}, \mathrm{z}, \mathrm{t}) = \eta(\mathrm{x}, \mathrm{y}, \mathrm{t}) - \mathrm{z} = 0 \tag{2.22}
$$

Where $\eta(\mathrm{x}, \mathrm{y}, \mathrm{t})$ denotes the surface elevation function. The kinetic boundary condition at free surface is the water particles must remain in the surface, which means the derivative of S should be zero. However, the Lagrangian derivative is adopted here instead of a partial derivative due to the point of interest is the change of the function S when one follows one given particle. The Lagrangian derivative is the derivative that follows the particle that describes the time rate of change of certain physical variables of an element that is subjected to a space-and-time-dependent velocity field variations of that physical variable, which is given by:

$$
\frac{\mathrm{D}}{\mathrm{D}\mathrm{t}} = \frac{\partial}{\partial \mathrm{t}} + \mathrm{u}_\mathrm{x}\frac{\partial}{\partial \mathrm{x}} + \mathrm{u}_\mathrm{y}\frac{\partial}{\partial \mathrm{y}} + \mathrm{u}_\mathrm{z}\frac{\partial}{\partial \mathrm{z}} \tag{2.23}
$$

Where u_x is the flow velocity that equals to $\frac{\partial \Phi}{\partial \mathrm{x}}$. Solving the Lagrangian derivative of surface function $\mathrm{S}(\mathrm{x}, \mathrm{y}, \mathrm{z}, \mathrm{t})$ to obtain the kinetic boundary condition at the free face as follows:

$$\frac{\partial \eta}{\partial t} + u_x \frac{\partial \eta}{\partial x} + u_y \frac{\partial \eta}{\partial y} = u_z \quad \text{at } z = \eta \tag{2.24}$$

The dynamic boundary condition is the pressure on the particle at free surface atmospheric is equivalent to atmospheric pressure:

$$p = p_{atmospheric} \tag{2.25}$$

Applying above to Bernoulli equation (see Appendix A):

$$\frac{\partial \Phi}{\partial t} + \frac{1}{2}\left({u_x}^2 + {u_y}^2 + {u_z}^2\right) + \frac{p_{atmospheric}}{\rho} + g\eta = 0 \tag{2.26}$$

Since the waves have a small steepness, the particle velocities u_x, u_y and u_z are small, this equation becomes:

$$\frac{\partial \Phi}{\partial t} + \frac{p_{atmospheric}}{\rho} + g\eta = 0 \tag{2.27}$$

The constant value $\frac{p_{atmospheric}}{\rho}$ can be included in $\frac{\partial \Phi}{\partial t}$. This will not affect the velocities being obtained from the potential Φ. With this equation becomes:

$$\frac{\partial \Phi}{\partial t} + g\eta = 0 \quad at\ z = \eta \tag{2.28}$$

The potential at the free surface can expand in a Taylor series, noting that vertical displacement is quite small:

$$\{\Phi\}_{z=\eta} = \{\Phi\}_{z=0} + \eta \cdot \left\{\frac{\partial \Phi}{\partial z}\right\}_{z=0} + \cdots + \left\{\frac{\partial \Phi}{\partial t}\right\}_{z=\eta} = \left\{\frac{\partial \Phi}{\partial t}\right\}_{z=0} + O(\epsilon^2) \tag{2.29}$$

Thus, the dynamic boundary conditions at the mean water surface are

$$\frac{\partial \Phi}{\partial t} + g\eta = 0 \quad \text{at } z = 0 \tag{2.30}$$

3. Radiation condition:

Since there is no disturbance due to floating body's presence:

$$\lim_{R \to \infty} \Phi = 0 \tag{2.31}$$

Where R is the distance between the observation point and the floating body.

4. The boundary condition at the surface of the floating structure:

The boundary condition at the surface of the structure will have to imply that the surface is watertight, say in other words: the velocity of the flow in the direction normal to the floating island has to be equal to the velocity of the floating island itself in normal direction when the island moves in the water, which can be written as:

$$\frac{\partial \Phi_j}{\partial n} = v_{nj} \tag{2.32}$$

Again, $j = 3,4,5$ are associated with three motion modes of the floating island.

The velocity of the floating island itself in the normal direction is:

$$v_{nj} = \dot{\zeta}_j \cdot f_j \tag{2.33}$$

Where $\dot{\zeta}_j$ is the oscillatory velocity of the given motion and f_j (which is the replacement for the body's normal vector pointing into the water n_k in equation 2.18) denotes the generalized direction cosine on the surface of the structure, S_0, given by:

$$\begin{aligned}
&\text{surge:} && f_1 = \cos(n,x)\\
&\text{sway:} && f_2 = \cos(n,y)\\
&\text{heave:} && f_3 = \cos(n,z)\\
&\text{roll:} && f_4 = \mathrm{y}f_3 - zf_2\\
&\text{pitch:} && f_5 = \mathrm{z}f_1 - xf_3\\
&\text{yaw:} && f_6 = \mathrm{x}f_2 - yf_1
\end{aligned} \tag{2.34}$$

A linear potential Φ in regular waves can be written as a product of a space-dependent term and a time-dependent harmonic term as follows:

$$\Phi(\mathrm{x},\mathrm{y},\mathrm{z},\mathrm{t}) = \phi(\mathrm{x},\mathrm{y},\mathrm{z}) \cdot e^{-i\omega t} \tag{2.35}$$

Therefore, the velocity of flow in a normal direction can be written as:

$$\frac{\partial \Phi_j}{\partial n} = \frac{\partial \phi_j}{\partial n} \cdot \dot{\zeta}_j \tag{2.36}$$

Combing equation 2.33, 2.35 and 2.36 provides the boundary condition at the surface of the floating body:

$$\frac{\partial \phi_j}{\partial n} = f_j \tag{2.37}$$

This boundary condition is the key to solve the radiation potentials.

2.3.4.2 Solving the radiation potentials

The problem of making the flow caused by a point source satisfies these boundary conditions, has been solved by (Lamb, 1932). It appears that so-called Green's function G can be derived that in view of these boundary conditions, enabling to write the potential ϕ_j at a point (x,y,z) on the mean wetted bottom surface S_0 resulting from a motion in the mode j (j=3,4,5) due to a continuous distribution of sources over a surface as:

$$\phi_j(x,y,z) = \frac{1}{4\pi} \iint_{S_0} \sigma_j(\hat{x},\hat{y},\hat{z}) \cdot G(x,y,z,\hat{x},\hat{y},\hat{z}) dS_0 \tag{2.38}$$

Where $\phi_j(x,y,z)$ is the potential function in a point (x,y,z) that refers to the location where the value of potential is evaluated on the mean wetted bottom surface. Similarly, $j = 3,4,5$ are associated with six motion modes. $(\hat{x},\hat{y},\hat{z})$ refers to the location of the source with strength $\sigma_j(\hat{x},\hat{y},\hat{z})$, which is the complex source strength in a point $(\hat{x},\hat{y},\hat{z})$. $G(x,y,z,\hat{x},\hat{y},\hat{z})$ is the so-called Green's function of pulsating source $\sigma_j(\hat{x},\hat{y},\hat{z})$ in a point located at $(\hat{x},\hat{y},\hat{z})$ on the potential $\phi_\mathrm{j}(\mathrm{x},\mathrm{y},\mathrm{z})$ in a point located at $(\mathrm{x},\mathrm{y},\mathrm{z})$, singular for $(\hat{\mathrm{x}},\hat{\mathrm{y}},\hat{\mathrm{z}}) = (\mathrm{x},\mathrm{y},\mathrm{z})$.

Substituting the expression for the $\phi_j(x,y,z)$ in the boundary condition for the radiation potential (equation 2.37) yields:

$$\frac{\partial(\frac{1}{4\pi}\iint_{S_0}\sigma_j(\hat{x},\hat{y},\hat{z})\cdot G(x,y,z,\hat{x},\hat{y},\hat{z})dS_0)}{\partial n} = f_j \qquad (2.39)$$

However, a problem appears for the point $(\mathrm{x},\mathrm{y},\mathrm{z})$ that coincides with $(\hat{\mathrm{x}},\hat{\mathrm{y}},\hat{\mathrm{z}})$, the potential at the location itself due to its singularity need to be addressed. Mathematically, a so-called principle value integral that excludes the singular point:

$$\frac{\partial\phi_j(x,y,z)}{\partial n} = -\frac{1}{2}\sigma_j(x,y,z) + \frac{1}{4\pi}\iint_{S_0}\sigma_j(\hat{x},\hat{y},\hat{z})\cdot\frac{\partial G(x,y,z,\hat{x},\hat{y},\hat{z})}{\partial n}dS_0 \quad (2.40)$$

The numerical approach of the equation, in this case, is to describe the shell of the floating island by flat panels and take for each of these panels a constant source strength, and select one point per panel (centroid of the panel) where we will satisfy the boundary condition. This point goes by the name of collection point m.

To ensure the feasibility and accuracy of the calculation at the same time, the bottom plane of the floating island, in this case, has been divided into 16 identical triangular panels that are shown in figure 2.4. The coordinate of the centroid of panel n is $(x_{pn}, y_{pn}, 0)$.

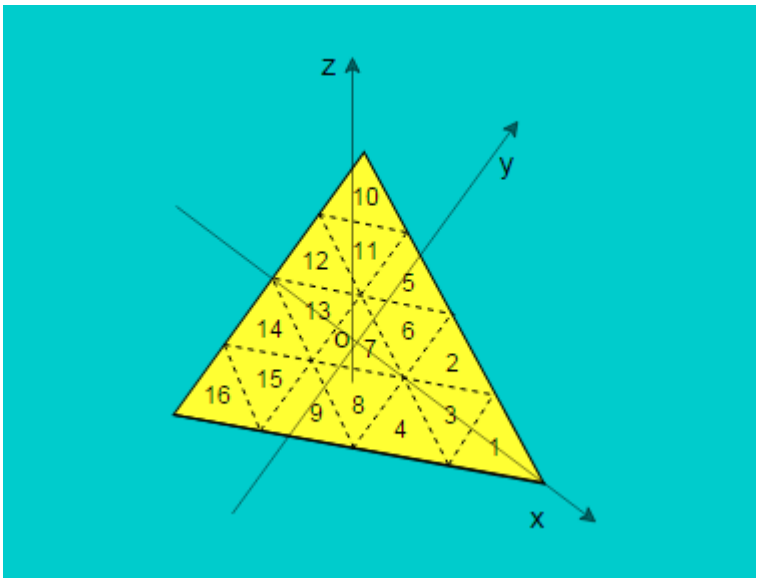

Figure 2.4: Panels on the bottom plane

Then, the normal derivative of potential at the location at (x,y,z), or$m$ as just defined, can be rewritten as follows:

$$\frac{\partial\phi_{mj}}{\partial n} = -\frac{1}{2}\sigma_{mj} + \frac{1}{4\pi}\sum_{n=1}^{16}\sigma_{nj}\cdot\frac{\partial G_{mn}}{\partial n}\Delta S_n \qquad (2.41)$$

Substituting it back in the boundary condition:

$$-\frac{1}{2}\sigma_{mj}+\frac{1}{4\pi}\sum_{n=1}^{16}\sigma_{nj}\cdot\frac{\partial G_{mn}}{\partial n}\Delta S_n=f_{mj} \tag{2.42}$$

There are 16 equations because the boundary condition must be satisfied with the collection points of all the 16 panels. There are also 16 unknowns due to each panel has its own source strength. Hence, the system of equations for solving the source strength for the radiation potential becomes:

$$\begin{bmatrix} A_{11} & \cdots & A_{1,16} \\ \vdots & \ddots & \vdots \\ A_{16,1} & \cdots & A_{16,16} \end{bmatrix}\cdot\begin{bmatrix} \sigma_{1,j} \\ \vdots \\ \sigma_{16,j} \end{bmatrix}=\begin{bmatrix} (f_j)_1 \\ \vdots \\ (f_j)_{16} \end{bmatrix} \tag{2.43}$$

Where:

$j = 3,4,5 = the\ radiation\ potential\ that\ is\ considered$

$A_{nn}=-\frac{1}{2}=influence\ of\ source\ at\ panel\ n\ on\ \frac{\partial\phi_j}{\partial n}\ at\ its\ own\ collocation\ point,$

$(n = 1,2,\dots 16)$

$A_{mn}=\frac{1}{4\pi}\frac{\partial G_{mn}}{\partial n}\Delta S_n=influence\ of\ source\ at\ panel\ n\ on\ \frac{\partial\phi_j}{\partial n}\ at\ collection\ point\ m,$

$(m = 1,2,\dots 16)$

$\sigma_{n,j} = unknown\ source\ strength\ of\ radiation\ potential\ (j = 3,4,5)\ at\ panel\ n$

$(f_j)_m = local\ normal\ direction\ due\ to\ motion\ in\ direction\ j\ at\ panel\ n$

Green's function:

To solve the unknown source strength $\sigma_{n,j}$, the Green's function has to be addressed, which is given by (Wehausen and Laitone, 1960):

$$G(x,y,z,\hat{x},\hat{y},\hat{z})\ according\ to\ [Wehausen\ and\ Laitone, 1960] =$$

$$\frac{1}{r}+\frac{1}{r_1}+PV\int_0^\infty\frac{2(\xi+\nu)e^{-\xi d}\cdot\cosh\xi(d_0+\hat{z})\cdot\cosh\xi(d_0+z)}{\xi\sinh\xi d-\upsilon\cosh\xi d}\cdot J_0(\xi R)\cdot d\xi$$

$$+i\cdot\frac{2\pi(k^2-\upsilon^2)\cdot\cosh k(d_0+\hat{z})\cdot\cosh k(d_0+z)}{(k^2-\upsilon^2)d-\nu}\cdot J_0(kR) \tag{2.44}$$

Where:

$$r=\sqrt{(x-\hat{x})^2+(y-\hat{y})^2+(z-\hat{z})^2}$$

$$r_1=\sqrt{(x-\hat{x})^2+(y-\hat{y})^2+(z+2+\hat{z})^2}$$

$$R=\sqrt{(x-\hat{x})^2+(y-\hat{y})^2}$$

$d = water\ depth$

$d_0 = distance\ from\ the\ origin\ to\ the\ seabed$

$\xi = a\ variable$

$\nu\cdot g = gk\tanh kd =\ the\ \ dispersion\ relationship$

$J_0 = Bessel\ function\ of\ the\ first\ kind\ for\ integer\ order\ \alpha = 0$

Note that the dispersion relationship is an implicit expression, A good alternative to use an explicit expression that approximates the solution is given by (Holthuijsen, 2007):

$$kd \approx \alpha(\tanh \alpha)^{-\frac{1}{2}} \quad with \quad \alpha = k_0 d = \frac{\omega^2 d}{g} \tag{2.45}$$

Bessel function of the first kind:

$$J(x) = \sum_{m=0}^{\infty} \frac{(-1)^m}{m!\,\Gamma(m+\alpha+1)} \left(\frac{x}{2}\right)^{(2m+\alpha)} \tag{2.46}$$

Where:
$\alpha = the\ order\ of\ the\ Bessel\ function, and\ \alpha = 0\ in\ this\ case$
$\Gamma(\mathrm{z})\ is\ the\ gamma\ function = (n-1)!$

To solve the Green's function, it can be divided into several parts, the part of principal value integral (real part) can be defined and named as $G_{r,int}$ as follows:

$$G_{r,int} = \int_0^{\infty} F(\xi) \cdot J_0(\xi R) \cdot d\xi \tag{2.47}$$

In which:

$$F(\xi) = \frac{2(\xi+\nu)e^{-\xi d} \cdot \cosh \xi(d_0+\hat{z}) \cdot \cosh \xi(d_0+z)}{\xi \sinh \xi d - \upsilon \cosh \xi d} \tag{2.48}$$

Correspondingly, the integrand of $G_{r,int}$ can be named as G_{real}:

$$G_{real} = F(\xi) \cdot J_0(\xi R) \tag{2.49}$$

Analogously, the imaginary part of the Green's function can be defined and named as G_{imag} as follows:

$$G_{imag} = \frac{2\pi(k^2-\upsilon^2) \cdot \cosh k(d_0+\hat{z}) \cdot \cosh k(d_0+z)}{(k^2-\upsilon^2)d - \nu} \cdot J_0(kR) \tag{2.50}$$

To make those two parts in Green's function, G_{real} and G_{imag}, more intuitive, the G_{real} curve that varied with ξ when R=8 and the G_{imag} curve that varied with R are illustrated in figure 2.5 and 2.6 separately.

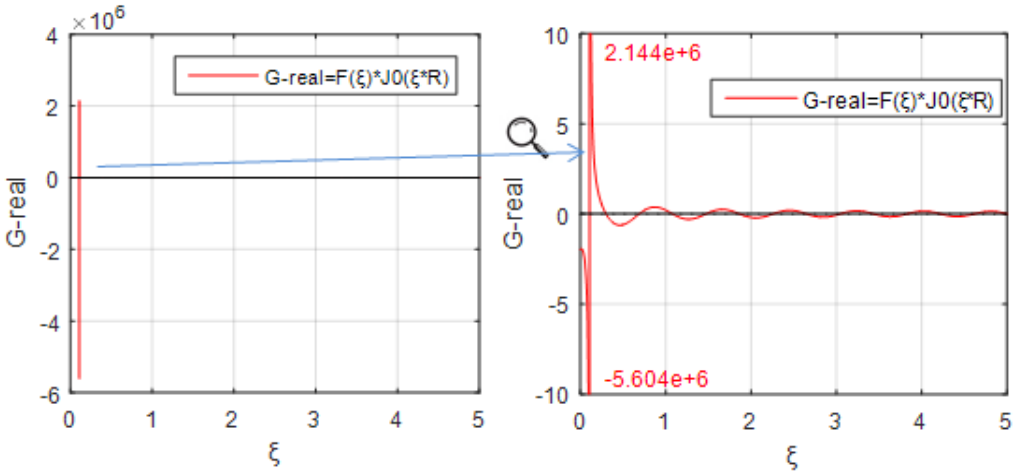

Figure 2.5: G_{real} varied with ξ

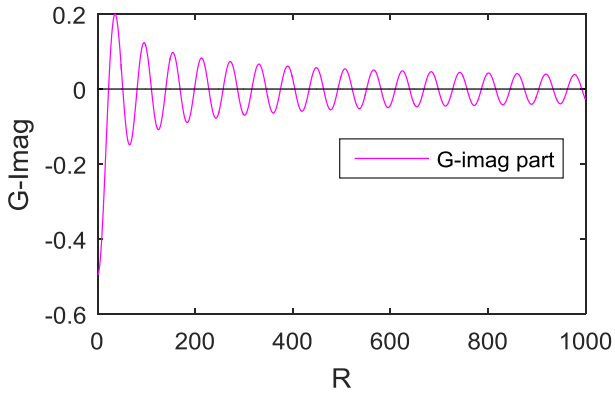

Figure 2.6: G_{imag} varied with R

It is clear to see that there is a huge jump existing at the singular point in function $\mathrm{G_{real}}$, which is the integrand of $\mathrm{G_{r,int}}$. To address this principle value integral in the Green's function, some simplifications have been implemented. Since in this case, $\mathrm{d_0 = d = 80\ (m)}$ and $\hat{\mathrm{z}} = \mathrm{z} = 0$ in the previous assumption, function $F(\xi)$ in equation 2.49 can be rewritten as follows:

$$F(\xi) = \frac{2(\xi + \nu)e^{-\xi d} \cdot \cosh(\xi d) \cdot \cosh(\xi d)}{\xi \sinh \xi d - \nu \cosh \xi d} \tag{2.51}$$

By the definition of the hyperbolic function:

$$\sinh \xi d = \frac{e^{\xi d} - e^{-\xi d}}{2} \quad and \quad \cosh \xi d = \frac{e^{\xi d} + e^{-\xi d}}{2} \tag{2.52}$$

For $\xi = 1$ and $\mathrm{d} = 80$:

$$\frac{e^{80} - e^{-80}}{2} \approx \frac{e^{\xi d}}{2} \quad and \quad \frac{e^{80} + e^{-80}}{2} \approx \frac{e^{\xi d}}{2} \tag{2.53}$$

Thus, for $\xi > 1$:

$$F(\xi) = \frac{2(\xi + \nu)e^{-\xi d} \cdot \frac{e^{2\xi d}}{4}}{\xi \frac{e^{\xi d}}{2} - \nu \frac{e^{\xi d}}{2}} = \frac{\xi + \nu}{\xi - \nu} \tag{2.54}$$

Hence, the function $G_{r,int}$ can be rewritten as:

$$G_{r,int} = \int_0^{\xi=1} F(\xi) \cdot J_0(\xi R) \cdot d\xi + \int_{\xi=1}^{\infty} \frac{\xi + \nu}{\xi - \nu} \cdot J_0(\xi R) \cdot d\xi \tag{2.55}$$

Since $\nu = k \tanh kd < 1$ and $F(\xi)$ is singular at $\xi = \nu$:

$$G_{r,int} = \int_0^{k \tanh kd} F(\xi) \cdot J_0(\xi R) \cdot d\xi + \int_{k \tanh kd}^{1} F(\xi) \cdot J_0(\xi R) \cdot d\xi + \int_1^{\infty} \frac{\xi + \nu}{\xi - \nu} \cdot J_0(\xi R) \cdot d\xi \tag{2.56}$$

For the last part of equation 2.55:

$$\int_1^{\infty} \frac{\xi + \nu}{\xi - \nu} \cdot J_0(\xi R) \cdot d\xi \approx \int_1^{10} \frac{\xi + \nu}{\xi - \nu} \cdot J_0(\xi R) \cdot d\xi + \int_{10}^{\infty} J_0(\xi R) \cdot d\xi$$
$$= \int_1^{10} \frac{\xi + \nu}{\xi - \nu} \cdot J_0(\xi R) \cdot d\xi + \frac{1}{R} - \int_0^{10} J_0(\xi R) \cdot d\xi \tag{2.57}$$

Therefore, the singular integral equation $G_{r,int}$ can be rewritten as:

$$G_{r,int} = \int_0^{\infty} F(\xi) \cdot J_0(\xi R) \cdot d\xi$$
$$= \frac{1}{R} + \int_0^{k \tanh kd \cdot 0.999} (F(\xi) - 1) \cdot J_0(\xi R) \cdot d\xi + \int_{k \tanh kd \cdot 1.001}^{1} (F(\xi) - 1) \cdot J_0(\xi R) \cdot d\xi + \int_1^{10} (\frac{\xi + \nu}{\xi - \nu} - 1) \cdot J_0(\xi R) \cdot d\xi \tag{2.58}$$

Now, the problem of a singular point in Green's function has been solved. The horizontal distance between field point and source point, R, can be calculated by the coordinates of panels as just defined. Then, a 16-by-16 matrix of Green's function is obtained.

Based on the equation 2.17, 2.18 and the assumption that the bottom plane is the only plane considered for hydrodynamic effect, hence heave, roll and pitch ($j = 3,4,5$) radiation potential are the only three radiation potentials need to be solved.

On the bottom plane:

$$\frac{\partial \phi_j}{\partial n} = \frac{\partial \phi_j}{\partial z}$$
$$\frac{\partial G_{mn}}{\partial n} = \frac{\partial G_{mn}}{\partial z} \tag{2.59}$$

The local normal direction due to the heave, roll and pitch at panel 1,2,…16:

$$(f_3)_1 = (f_3)_2 = \cdots = (f_3)_{16=} - 1$$
$$(f_4)_1 = -y_{p1}, (f_4)_2 = -y_{p2}, \ldots = (f_4)_{16=} - y_{p16}$$
$$(f_5)_1 = x_{p1}, (f_3)_2 = x_{p2}, \ldots = (f_5)_{16=} x_{p16} \quad (2.60)$$

Again, $(x_{pn}, y_{pn}, 0)$ is the coordinate of centroid of panel n.

Substituting the results of Green's function and above equations in the following boundary condition to solve the source strength $\sigma_{n,j}$:

$$\begin{bmatrix} A_{11} & \cdots & A_{1,16} \\ \vdots & \ddots & \vdots \\ A_{16,1} & \cdots & A_{16,16} \end{bmatrix} \cdot \begin{bmatrix} \sigma_{1,j} \\ \vdots \\ \sigma_{16,j} \end{bmatrix} = \begin{bmatrix} (f_j)_1 \\ \vdots \\ (f_j)_{16} \end{bmatrix} \quad (2.61)$$

Then, the heave, roll and pitch radiation potentials can be solved by:

$$\phi_j(x,y) = \sum_{n=1}^{16} \phi_{n,j}(x,y,z) = \sum_{n=1}^{16} \frac{1}{4\pi} \iint_{S_0} \sigma_{n,j}(\hat{x},\hat{y}) \cdot G(x,y,\hat{x},\hat{y}) d\hat{x} d\hat{y} \quad (2.62)$$

Substituting the results of radiation potentials at different frequencies in equation 2.18 to obtain the added mass and damping coefficients for heave, roll, and pitch as a function of frequency separately. Again, the following symmetry relationships should be noticed:

$$a_{kj} = a_{jk}$$
$$b_{kj} = b_{jk} \quad (2.63)$$

The results of added masses and damping coefficients are shown in figure 2.7 and 2.8 respectively:

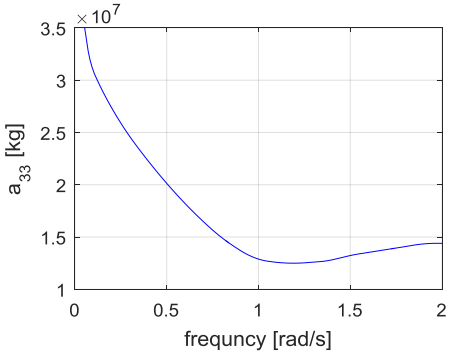

(a) a_{33}

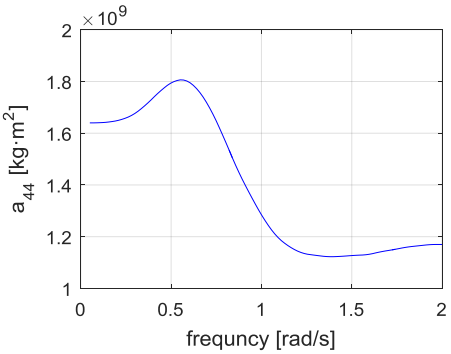

(b) a_{44}

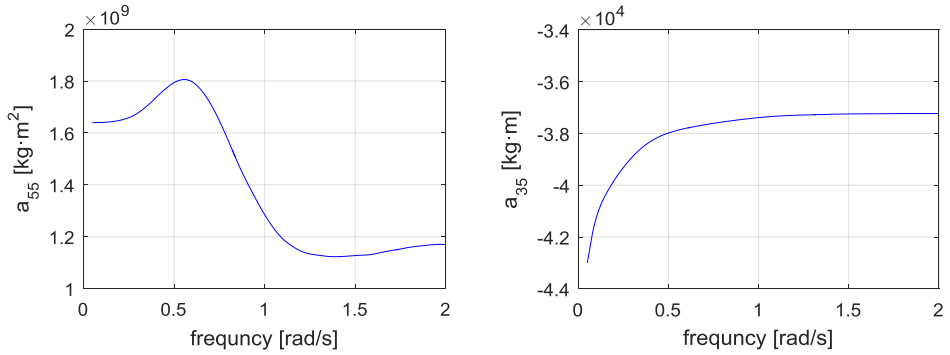

(a) a_{55} (b) a_{35}

Figure 2.7: Added mass for heave, roll and pitch

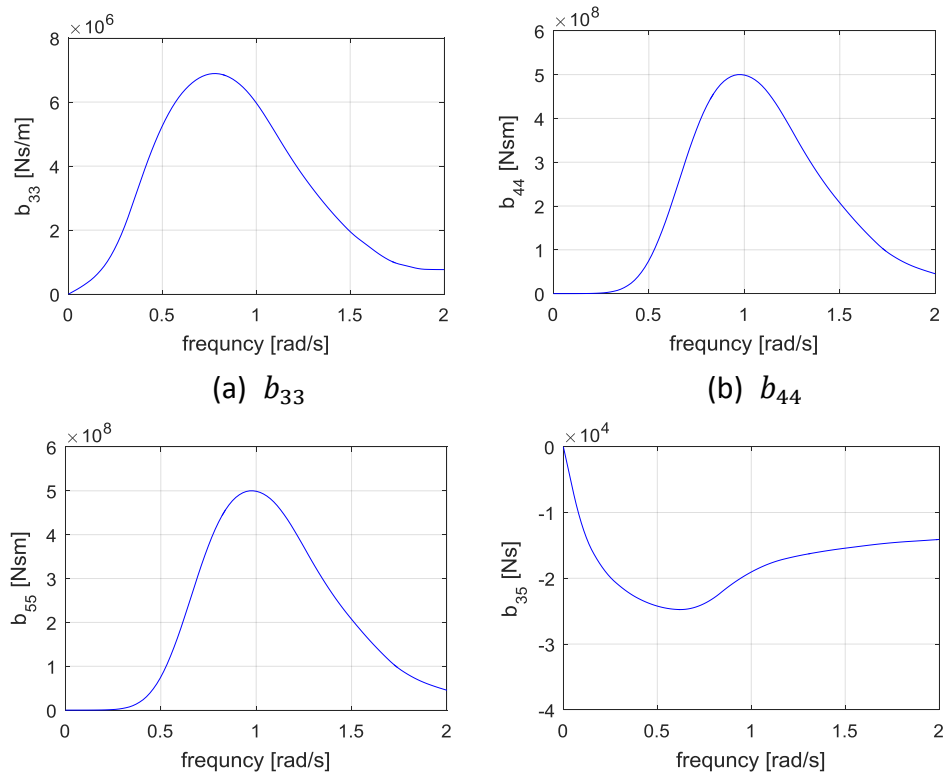

(a) b_{33} (b) b_{44}

(a) b_{33} (b) b_{35}

Figure 2.8: Damping coefficients for heave, roll and pitch

From figure 2.7, one can see that the added mass in heave goes logarithmically to infinity when the oscillating frequency approaches zero and these added masses approach the asymptotic values when the oscillating frequency approaches infinity.

From figure 2.8, one can see that the damping coefficients go toward zero for very low and very high frequencies, which are caused by the outgoing waves will not be generated when the frequency approaches zero or infinity, and the energy cannot be dissipated by radiation effect.

Besides the oscillating frequency and water depth, the added mass and damping

coefficients are strongly influenced by the body shape, which is also the reason why the numerical method has to be used to estimate the radiation forces. Another conclusion is the added mass and damping coefficients in rotational motions are much larger than that in translational movements, in other words, they are not on the same order of magnitude. Moreover, the increase of the added mass will reduce the natural frequency of the floating structure that raises the possibility of resonance, which should be avoided as far as possible in the design.

2.3.5 Wave excitation

Wave exciting forces are caused by the effect of the incident waves on the floating structures. The interactions between the exciting forces and the radiation forces are small that can be neglected in linear theory as assumed in this case. The wave exciting force of the floating body in regular waves can be split up into two parts: the Froude–Krylov force and the diffraction force.

2.3.5.1 Froude–Krylov force

The Froude–Krylov force is a hydrodynamical force formed by the undisturbed wave, assuming the water is not affected by the presence of the object. In case of potential flow, the forces on a floating body surrounded by the flow can only be a product of pressures in the water at the location of the shell of the floating body due to the inviscid flow, meaning the water can only exert a force perpendicularly to the shell of the floating body.

The pressure in the fluid follows from Bernoulli's equation:

$$p = -\rho \frac{\partial \Phi}{\partial \mathrm{t}} - \frac{1}{2}\rho\left({u_x}^2 + {u_\mathrm{y}}^2 + {u_\mathrm{z}}^2\right) - \rho g z \qquad (2.64)$$

The term $-\rho g z$ represents the hydrostatic pressure. The Integral of this term over the submerged shell of the floating island is the buoyancy force that forms a static equilibrium with the weight of the island and does not contribute to the dynamic behavior. The second term in equation 2.64 is non-linear. In line with the linearization that stated at the beginning of this section, $\mathrm{u_x}$, $\mathrm{u_y}$ and $\mathrm{u_z}$ are the wave-induced flow velocities in their respective directions. Linearizing the pressure means that all terms that are proportional to squares (or higher powers) of wave related properties (such as the particle velocities $\mathrm{u_x}$, $\mathrm{u_y}$ and $\mathrm{u_z}$) will be neglected. Hence the second pressure term in equation 2.64 will be neglected when considering linear dynamic behavior of this floating island in waves, and the first term is the only one that left. Note that $\Phi = \Phi_0$ when the undisturbed wave is considered here. Combining equation for the undisturbed wave potential and the conclusions above provide the linear unsteady pressure is:

$$p_0 = -\rho\frac{\partial\Phi_0}{\partial \mathrm{t}} = \rho\zeta_a\frac{\omega^2}{k}\frac{\cosh\big(k(d_0+z)\big)}{\sinh(kd)}\cos(kx\cos\mu + ky\sin\mu - \omega t) \quad (2.65)$$

The Froude–Krylov force and moment can be calculated as follows:

$$\vec{F}_{FK} = -\iint_{S_0}(p_0\cdot\vec{n})dS_0$$

$$\vec{M}_{FK} = -\iint_{S_0} p_0\cdot(\vec{r}\times\vec{n})dS_0 \quad (2.66)$$

Where:

S_0 = The area of the mean wetted surface $[\mathrm{m}^2]$

$\vec{r}$ = The location vector that is the three-component position vector indicating the x, y and z coordinate at the shell of the floating island.

$\vec{n}$ = The body's normal vector that is the three-component normal vector of unit length 1 whose direction is perpendicular to the shell of floating island pointing into the surrounding water

Again, the bottom plane is the only wetted surface will be considered for the hydrodynamic effect. Thus the Froude–Krylov forces only exist in heave, pitch and roll motions. Calculating them in the frequency domain and the results of the Froude–Krylov forces at various frequencies with angles of attack equal to $30°$, $45°$ and $60°$ are shown in figure 2.9 respectively.

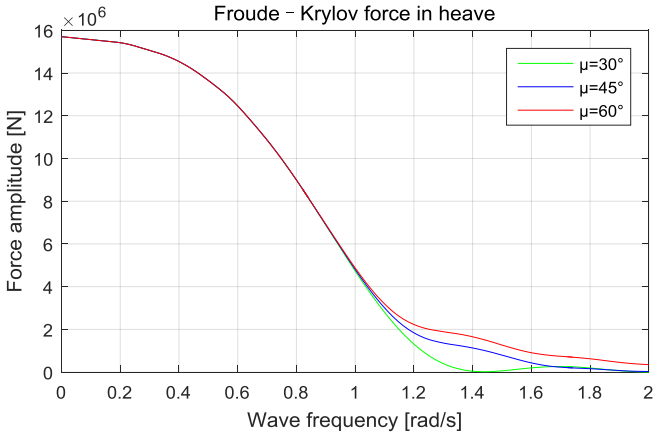

(a) Froude–Krylov force in heave

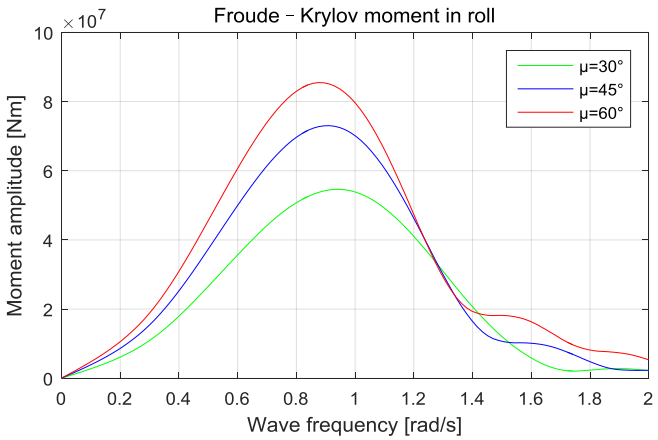

(b) Froude–Krylov moment in roll

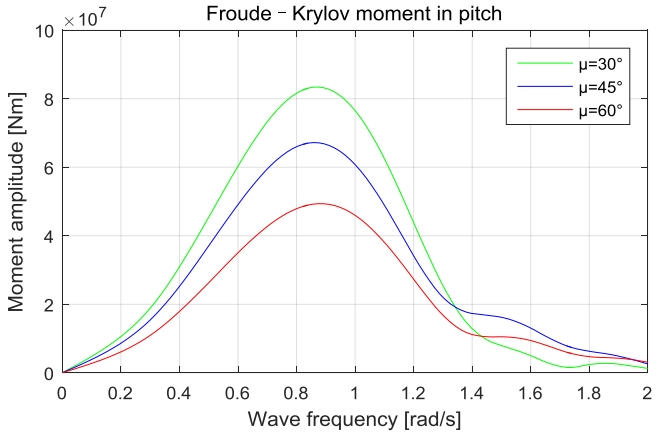

(c) Froude–Krylov moment in pitch

Figure 2.9: Froude–Krylov forces in three modes

From the above figures, one can see that the undisturbed wave force in heave motion tends to decline as the frequency increases, while the undisturbed wave moment in roll tends to rise first and then drop as the frequency increases, which is the same as that in pitch.

2.3.5.2 Boundary conditions for diffraction potential

The diffraction force is caused by the disturbance of the floating structure to the waves, as it is a correction on the undisturbed flow and thinks about the presence of the structure. This force is called the diffraction force and is indicated by F_D here. It is determined by diffraction potential function that is added to the existing regular wave potential. The undisturbed wave potential and diffraction potential together ensure that the normal velocity at the shell of the structure is zero. The hydrodynamic pressure due to the diffraction potential can be determined in accord with what was done for the undisturbed wave potential:

$$p_7 = \rho \frac{\partial \Phi_7}{\partial \mathrm{t}} \tag{2.67}$$

Then the diffraction force and moment can be calculated in the same way as that used for the Froude–Krylov forces as follows:

$$\vec{F}_D = -\iint_{S_0} (p_7 \cdot \vec{n}) dS_0$$

$$\vec{M}_D = -\iint_{S_0} p_7 \cdot (\vec{r} \times \vec{n}) dS_0 \tag{2.68}$$

The solve the diffraction potential Φ_7, the first three boundary conditions in section 2.3.4.1 must be satisfied again, which is the same as radiation potential in this respect. The watertight boundary condition, however, should be altered when considering the excitation due to waves: the resultant fluid velocity in the normal direction to the floating structure due to the incoming wave undisturbed wave potential and the diffraction potential should be zero:

$$\frac{\partial \Phi_0}{\partial n} + \frac{\partial \Phi_7}{\partial n} = 0 \tag{2.69}$$

After eliminating the time-dependent term:

$$\frac{\partial \phi_0}{\partial n} + \frac{\partial \phi_7}{\partial n} = 0$$

$$\frac{\partial \phi_7}{\partial n} = -\frac{\partial \phi_0}{\partial n} \tag{2.70}$$

2.3.5.3 Solving the diffraction potential

The approach to solving the diffraction potential is similar to what was used for solving the radiation potentials. The interface condition in equation 2.70 can be rewritten as:

$$\frac{\partial \phi_0}{\partial n} + \frac{\partial \phi_7}{\partial n} = 0$$

$$\frac{\partial \phi_0}{\partial n} + \frac{\partial (\frac{1}{4\pi} \iint_{S_0} \sigma_7(\hat{x}, \hat{y}, \hat{z}) \cdot G(x, y, z, \hat{x}, \hat{y}, \hat{z}) dS_0)}{\partial n} = 0$$

$$\frac{\partial \phi_0}{\partial n} - \frac{1}{2}\sigma_7(x, y, z) + \frac{1}{4\pi} \oiint_{S_0} \sigma_7(\hat{x}, \hat{y}, \hat{z}) \cdot \frac{\partial G(x, y, z, \hat{x}, \hat{y}, \hat{z})}{\partial n} dS_0$$

$$-\frac{1}{2}\sigma_{mj} + \frac{1}{4\pi} \sum_{n=1}^{N} \sigma_{n7} \cdot \frac{\partial G_{mn}}{\partial n} \Delta S_n = -\left(\frac{\partial \phi_0}{\partial n}\right)_m \tag{2.71}$$

Again, the bottom plane of the floating island has been divided into 16 identical triangular panels, which is identical to what was done for solving the radiation potentials in figure 2.4, the coordinate of the centroid of panel n is $(x_{pn}, y_{pn}, 0)$ as well, then the equation 2.71 can be rewritten as:

$$-\frac{1}{2}\sigma_{mj}+\frac{1}{4\pi}\sum_{n=1}^{16}\sigma_{n,7}\cdot\frac{\partial G_{mn}}{\partial n}\Delta S_n=-\left(\frac{\partial\phi_0}{\partial n}\right)_m \tag{2.72}$$

The system of equations for solving the source strength for the diffraction potential becomes:

$$\begin{bmatrix} A_{11} & \cdots & A_{1,16} \\ \vdots & \ddots & \vdots \\ A_{16,1} & \cdots & A_{16,16} \end{bmatrix}\cdot\begin{bmatrix} \sigma_{1,7} \\ \vdots \\ \sigma_{16,7} \end{bmatrix}=\begin{bmatrix} -\left(\frac{\partial\phi_0}{\partial n}\right)_1 \\ \vdots \\ -\left(\frac{\partial\phi_0}{\partial n}\right)_{16} \end{bmatrix} \tag{2.73}$$

Where:

$A_{nn}=-\frac{1}{2}=influence\ of\ source\ at\ panel\ n\ on\ \frac{\partial\phi_7}{\partial n}\ at\ its\ own\ collocation\ point,$
$(n=1,2,\dots 16)$

$A_{mn}=\frac{1}{4\pi}\frac{\partial G_{mn}}{\partial n}\Delta S_n=influence\ of\ source\ at\ panel\ n\ on\ \frac{\partial\phi_7}{\partial n}\ at\ collection\ point\ m,$
$(m=1,2,\dots 16)$

$\sigma_{n,7}=unknown\ source\ strength\ of\ diffraction\ potential\ \ at\ panel\ n$

Similarly, solving the Green's function and then obtaining the diffraction potential function $\phi_7(x,y)$:

$$\phi_7(x,y)=\sum_{n=1}^{16}\phi_{n,7}(x,y,z)=\sum_{n=1}^{16}\frac{1}{4\pi}\iint_{S_0}\sigma_{n,7}(\hat{x},\hat{y})\cdot G(x,y,\hat{x},\hat{y})d\hat{x}d\hat{y} \tag{2.74}$$

After substituting the results of diffraction potential at different frequencies in equation 2.68, the diffraction forces are obtained. Note that the bottom plane is the only plane was considered due to the assumption. Thus the diffraction forces only exist in heave, pitch and roll. The results of the diffraction forces at various frequencies with angles of attack equal to $30°$, $45°$ and $60°$ are shown in figure 2.10.

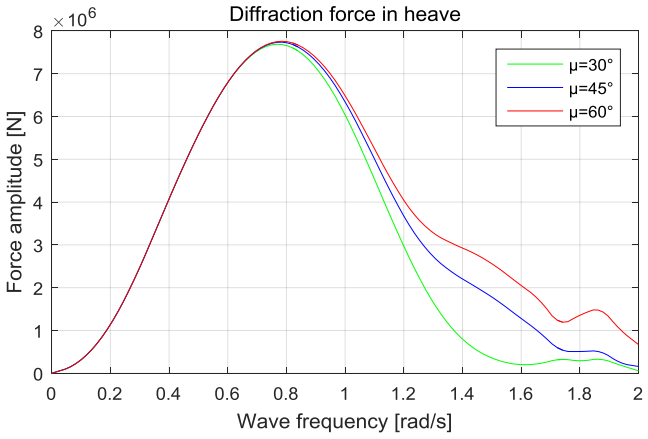

(a) Diffraction force in heave

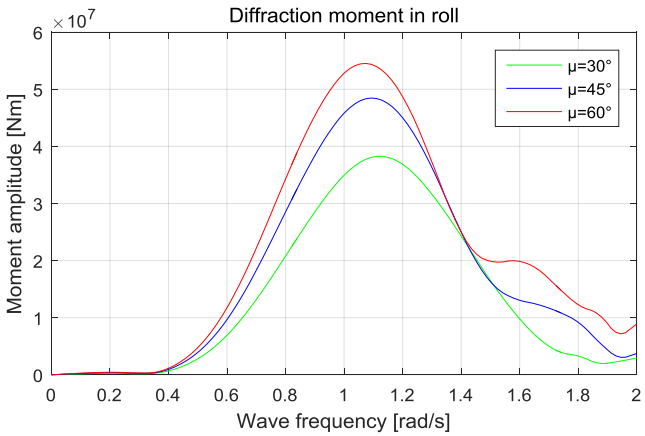

(b) Diffraction moment in roll

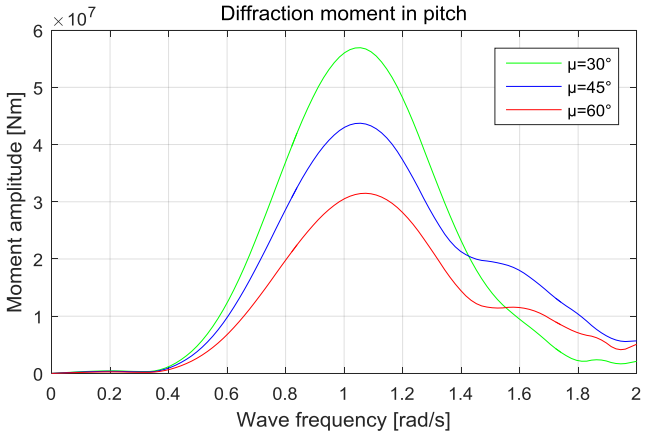

(c) Diffraction moment in pitch

Figure 2.10: Diffraction forces in three modes

From the above figures, one can see that the diffraction forces in both three modes are in the minimum condition when the wavelength is very long and very short.

2.3.5.4 Total wave exciting forces

Now, the expressions for the Froude–Krylov forces and diffraction forces are obtained. The entire wave exciting force can be expressed as the summation of these two parts:

$$F_{wave} = F_{FK} + F_D \tag{2.75}$$

The total wave exciting forces at various frequencies in heave, pitch and roll with angles of attack equal to $30°$, $45°$ and $60°$ are shown in figure 2.11.

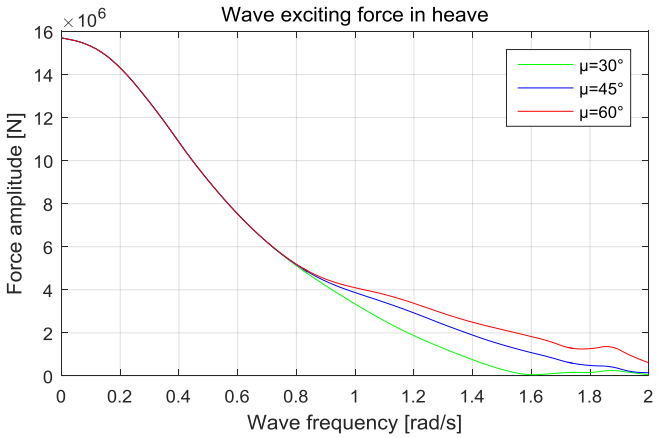

(a) Wave exciting forces in heave

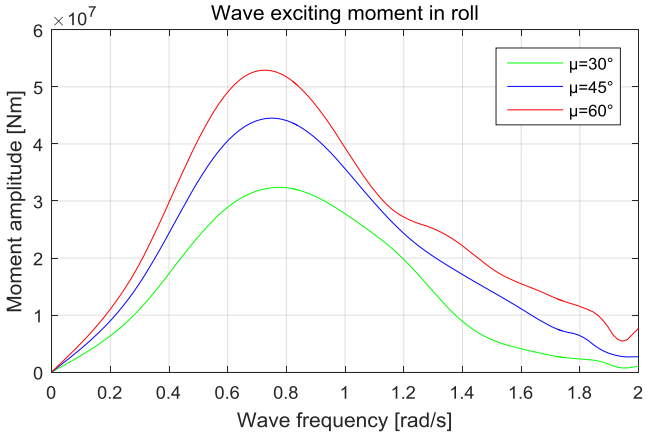

(b) Wave exciting moments in roll

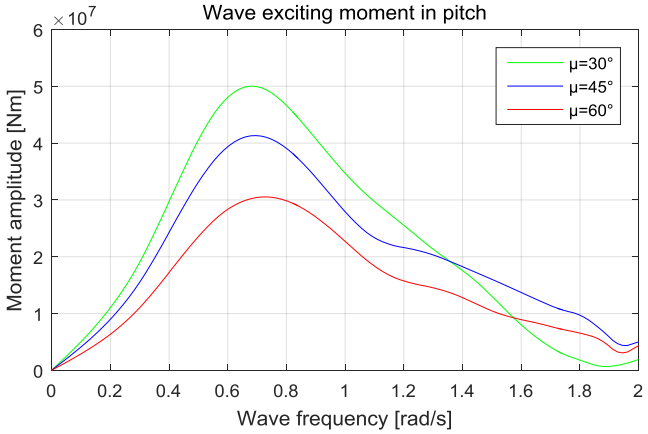

(c) Wave exciting moments in pitch

Figure 2.11: Total wave exciting forces in three modes

One can see that the amplitude and phase of the excitation force depend on encounter angle, wave frequency, size of the wetted surface, wave amplitude and water depth, and the amplitude variation of wave excitation forces is irrelative to the radiation forces.

2.3.6 Stiffness

Stiffness means the extent to which a body resists deformation in response to the force. It is a representation of the ease or complexity in elastic deformation of materials or structures. To calculate it, it is the proportional coefficient of the load to the displacement; in other words, it stands for the restoring force required to produce a unit displacement. In this chapter, this restoring force consists of hydrostatic effect, mooring forces and gravity.

The first step is to analyze the hydrostatic effect. For a ship in the free surface the only nonzero linear hydrostatic terms could be found as (Salvesen et al., 1970):

$$\boldsymbol{K}_{hydrostatic} = \begin{bmatrix} 0 & 0 & 0 & 0 & 0 & 0 \\ 0 & 0 & 0 & 0 & 0 & 0 \\ 0 & 0 & k_{33} & 0 & k_{35} & 0 \\ 0 & 0 & 0 & k_{44} & 0 & 0 \\ 0 & 0 & k_{53} & 0 & k_{55} & 0 \\ 0 & 0 & 0 & 0 & 0 & 0 \end{bmatrix} \tag{2.76}$$

Again, k_{ij} denotes the restoring force in i-direction due to the motion in j-direction. Each value in the hydrostatic stiffness matrix will be found individually in the following parts.

k_{33} represents the restoring coefficient in z-direction due to motion in the z-direction. This hydrostatic force can be expressed as:

$$F_{static33} = \rho_w g \nabla = \rho_w g A_{wl} z = \frac{\sqrt{3}}{4} \rho_w g s^2 z \tag{2.77}$$

Where:
$\rho_w = 1025$ The density of seawater $[kg/m^3]$
$g = 9.81$ The gravitational acceleration $[m/s^2]$
∇ = The volume of displacement $[m^3]$
A_{wl} = The water plane area $[m^2]$
s = The side length of the triangle $[m]$

In another hand, this hydrostatic force can be written in another form in the light of the Hooke's law:

$$F_{static33} = k_{33} z \tag{2.78}$$

Combining equation 2.78 and 2.79 provides the value of k_{33}:

$$k_{33} = \frac{\sqrt{3}}{4} \rho_w g s^2 \tag{2.79}$$

To calculate k_{35}, the pitch motion should be analyzed first. The real pitch motion is shown in figure 2.12, the green dotted line indicates the x-axis as well as the center line that goes through the COG before rotation, and the solid red line indicates the center line that goes through the COG after rotation. The triangle would turn around its center of floatation, which is maybe another vertical location than our origin but

the distance between the origin and center of floatation will not affect the stabilizing moment if we linearized, the restoring coefficient is indeed k_{35}.

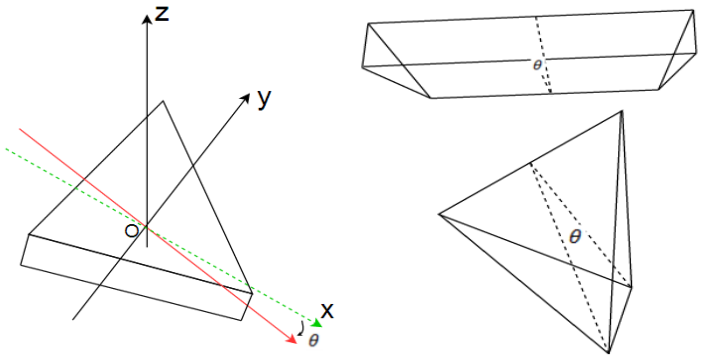

(a) Pitch (b) The amount of volume that was lost compared with the volume that was gained due to pitch

Figure 2.12: Pitch motion

One can calculate the amount of volume that was lost and that was gained depending on figure 2.12(b):

$$\nabla_{lose} = \frac{1}{2}\left(\frac{\sqrt{3}s}{6}\right)^2 \sin(\theta) \times \frac{2}{3}\mathrm{s} + 2 \times \frac{1}{3} \times \frac{\mathrm{s}}{6} \times \frac{1}{2} \times \frac{1}{2}\left(\frac{\sqrt{3}s}{6}\right)^2 \sin(\theta) = \frac{1}{27}s^3 \sin\theta \quad (2.80)$$

$$\nabla_{gain} = \frac{1}{6}\left|-\frac{\sqrt{3}s}{3} \times \frac{s}{3} \times \frac{\sqrt{3}s}{3}\sin\theta - \frac{\sqrt{3}s}{3} \times \frac{s}{3} \times \frac{\sqrt{3}s}{3}\sin\theta\right| = \frac{1}{27}s^3 \sin\theta \quad (2.81)$$

It can be clearly seen that the amount of volume that we gain is exactly equal to the volume that we lose, so the force that was gained is also equal to the force that was lost due to that is directly proportional to the volume, which means heave is not influenced by pitch. The conclusions for the above can be expressed as:

$$k_{35} = 0 \quad (2.82)$$

The value of k_{44} depends on the roll moment due to roll motion. A front view respects to the y-z plane when the triangle rotates an angle ϕ around the x-axis is shown in figure 2.13.

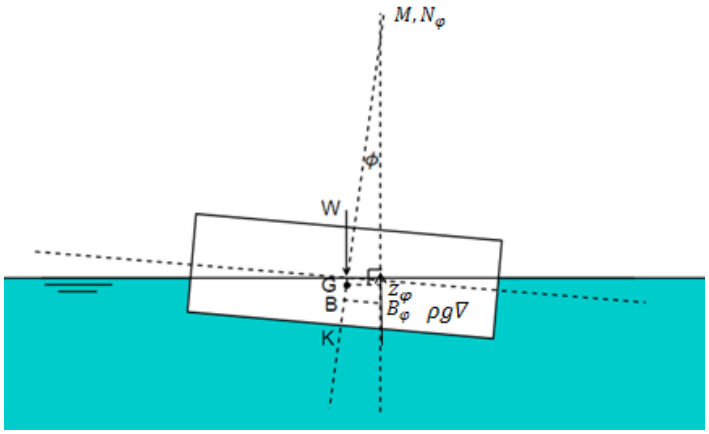

Figure 2.13: Hydrostatic restoring moment for roll

Thus, the roll restoring moment can be found as:

$$M_{static44} = \rho_w g \nabla \times GZ_\phi = \rho_w g \nabla \times GM \times \sin\varphi = M_{44} = k_{44}\varphi \qquad (2.83)$$

The final equations of motion are always linearized by assuming that rotational angles are small. To simplify the equations of motion and keep the result's accuracy, the first few terms of Taylor series of sine and cosine angles can be used.

$$sin\,\varphi = \varphi - \frac{\varphi^3}{3!} + \frac{\varphi^5}{5!} - \cdots \approx \varphi - O(\varphi^3) + O(\varphi^5) \Rightarrow sin\,\varphi \approx \varphi$$

$$\cos\varphi = 1 - \frac{\varphi^2}{2!} + \frac{\varphi^4}{4!} - \cdots \approx 1 - \frac{\varphi^2}{2} + O(\varphi^4) \Rightarrow \cos\varphi \approx 1 \qquad (2.84)$$

As mentioned above, those approximate values can only be made when the rotational angles are small enough. When the angle closes to zero, one can see that the gap between two curves vanishes. This phenomenon is shown in figure 2.14.

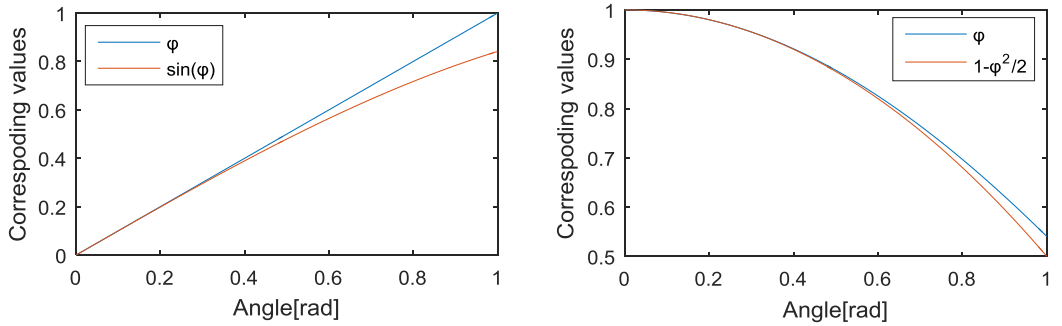

(a) A comparison of φ and $\sin\varphi$ (b) A comparison of $\cos\varphi$ and $1 - \frac{\varphi^2}{2}$

Figure 2.14: The accuracy of the linear approximation

In this project, the rotational angle is quite small. On the premise that the numerical results are almost unaffected by this small factor, this approximation will be implemented.

Thus, the relation between roll moments and angle can be simplified as:

$$M_{static44} = \rho_w g \nabla \times GZ_\phi = \rho_w g \nabla \times GM \times \varphi \qquad (2.85)$$

Additionally, M and N_ϕ can be considered as the same point in linear theory that is called the metacenter. GM is the metacenter height that is expressed as:

$$GM = KB + BM - KG \qquad (2.86)$$

In which KB is the height of the center of buoyancy and KG is the height of the center of gravity, which is two straightforward values. BM represents the initial metacentric radius that is a more complicated value determined by the shift of the center of buoyancy as:

$$BB_\varphi = \frac{2\int_0^L 1/3\, y^3 dx}{\nabla} tan\phi$$

$$BM = \frac{BB_{\phi}}{tan\phi} = \frac{I_t}{\nabla} \tag{2.87}$$

The term I_t represents the moment of inertia of the waterplane area. For this case:

$$I_t = \frac{\sqrt{3}s^4}{96} \tag{2.88}$$

Substituting equations 2.86, 2.87, and 2.88 in equation 2.85, k_{44} is rewritten as:

$$k_{44} = \rho_w g \left(\frac{\sqrt{3}}{4} s^2 \mathrm{T}\right)\left(\frac{T}{2} + \frac{s^2}{24T} - \frac{h}{2}\right) \tag{2.89}$$

Where T is the draft of the triangle

Similarly, k_{55} can be calculated in the same way as that for k_{44}.

$$k_{55} = \rho_w g \left(\frac{\sqrt{3}}{4} s^2 \mathrm{T}\right)\left(\frac{T}{2} + \frac{s^2}{24T} - \frac{h}{2}\right) \tag{2.90}$$

k_{53} is zero. No pitch moment is generated due to heave motion because the center of gravity and the center of floatation are always aligned since the triangle is a regular triangular prism, the pitch lever and its moment are all zero.

$$k_{53} = 0 \tag{2.91}$$

From the above, the potential energy due to the hydrostatic effect can be found as:

$$V_{hs3} = \frac{1}{2} k_{33} z^2$$

$$V_{hs4} = \frac{1}{2} k_{44} \varphi^2$$

$$V_{hs5} = \frac{1}{2} k_{55} \theta^2 \tag{2.92}$$

The potential energy due to gravity:

$$V_g = mgz \tag{2.93}$$

Based on the configuration of mooring lines (see figure 2.3), the potential energy due to mooring springs:

$$V_{moor1} = \frac{1}{2} k_0 [x + \frac{\sqrt{3}s}{3}(1 - \cos\theta) + \frac{\sqrt{3}s}{3}(1 - \cos\psi)]^2$$

$$V_{moor2} = \frac{1}{2} k_0 (-x\cos 60° - y\cos 30° + \frac{s}{2}(1 - \cos\varphi)\cos 30° + \frac{\sqrt{3}s}{6}(1 - \cos\theta)\cos 60° + \frac{\sqrt{3}s}{3}(1 - \cos\psi))^2$$

$$V_{moor3} = \frac{1}{2} k_0 (-x\cos 60° + y\cos 30° + \frac{s}{2}(1 - \cos\varphi)\cos 30° + \frac{\sqrt{3}s}{6}(1 - \cos\theta)\cos 60° + \frac{\sqrt{3}s}{3}(1 - \cos\psi))^2$$

$$V_{moor4} = \tfrac{1}{2} k_r \psi^2 \tag{2.94}$$

Where:

$k_0 = horizontal\ mooring\ stiffness\ coefficient = 1.567 * 10^7\ (N/m)$

$k_r = \ rotational\ mooring\ stiffness\ coefficient = 2.226 * 10^9\ (Nm)$

The value of k_0 and k_r are determined by the value of hydrostatic stiffness

coefficient k_{33} and k_{44} respectively:

$$k_0 = k_{33} \quad and \quad k_r = k_{44} \tag{2.95}$$

As previously explained, the hydrodynamic forces on the broadsides are much smaller than that on the bottom plane. Thus the motions due to the hydrodynamic effect on the broadsides are small as well if the stiffness in surge and sway is the same as that in heave.

In summary, the total potential energy becomes:

$$V = V_{hs3} + V_{hs4} + V_{hs5} + V_g + V_{moor1} + V_{moor2} + V_{moor3} + V_{moor4} \tag{2.96}$$

2.4 Modelling results

The generalized force Q_i equals to total wave exciting force in this project:

$$Q_i = F_{wave,i} \tag{2.97}$$

After substituting all the above results of kinetic energies, potential energies and the generalized forces in the Euler-Lagrange equation, it can be rewritten as:

$$\frac{d}{dt}\left(\frac{\partial T}{\partial \dot{x}_i}\right) + \frac{\partial D}{\partial \dot{x}_i} - \frac{\partial V}{\partial x_i} = Q_i \tag{2.98}$$

Note that the small angle approximation is implemented after one solved the derivative of potential energy with respect to time. Next, the equations of motion for the bottom plane of this floating island can be expressed as:

$$(\boldsymbol{M} + \boldsymbol{A})\ddot{\boldsymbol{x}} + \boldsymbol{B}\dot{\boldsymbol{x}} + \boldsymbol{K}\boldsymbol{x} = \boldsymbol{Q} \tag{2.99}$$

Where:

$$\boldsymbol{x} = [z \quad \phi \quad \theta]^T \qquad \dot{\boldsymbol{x}} = [\dot{z} \quad \dot{\phi} \quad \dot{\theta}]^T \qquad \ddot{\boldsymbol{x}} = [\ddot{z} \quad \ddot{\phi} \quad \ddot{\theta}]^T$$

$$\boldsymbol{M} = \begin{bmatrix} m & 0 & 0 \\ 0 & J_4 & 0 \\ 0 & 0 & J_5 \end{bmatrix} \quad \boldsymbol{A} = \begin{bmatrix} a_{33} & 0 & a_{35} \\ 0 & a_{44} & 0 \\ a_{53} & 0 & a_{55} \end{bmatrix} \quad \boldsymbol{B} = \begin{bmatrix} b_{33} & 0 & b_{35} \\ 0 & b_{44} & 0 \\ b_{53} & 0 & b_{55} \end{bmatrix}$$

$$\boldsymbol{K} = \begin{bmatrix} k_{33} & 0 & 0 \\ 0 & k_{44} & 0 \\ 0 & 0 & k_{55} \end{bmatrix} \qquad \boldsymbol{Q} = \begin{bmatrix} F_{FK3} + F_{D3} \\ F_{FK4} + F_{D4} \\ F_{FK5} + F_{D5} \end{bmatrix} \tag{2.100}$$

Generally speaking, $\boldsymbol{M}$ represents a generalized mass matrix. $\boldsymbol{A}$ represents the added mass matrix that is the inertia of some amount of surrounding fluid added to the system due to the floating body's acceleration or deceleration. $\boldsymbol{B}$ represents the radiation damping matrix that stands for the energy dissipation. $\boldsymbol{K}$ represents the stiffness matrix that shows the contributions of hydrostatic, mooring system and gravity effect in the system. $\boldsymbol{Q}$ is a generalized wave excitation acting along the generalized coordinate x.

The displacements in the frequency domain can be obtained by the amplitudes of displacements that were obtained in the time domain, the results with angles of attack equal to $30°$, $45°$ and $60°$ are shown in figure 2.15.

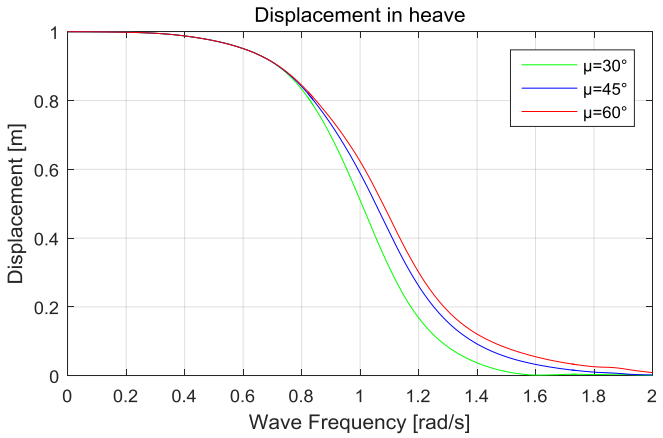

(a) Heave displacement

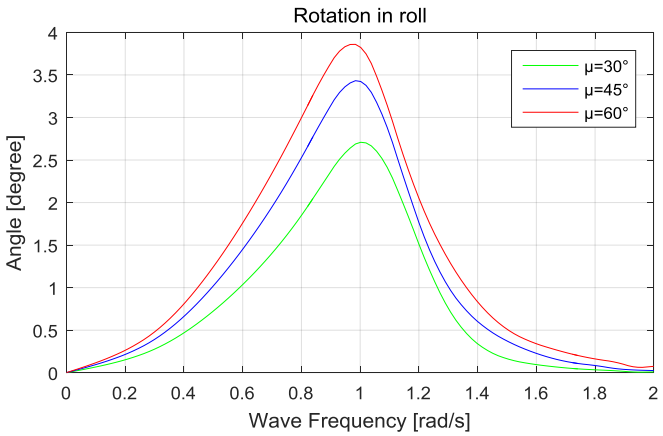

(b) Roll angle

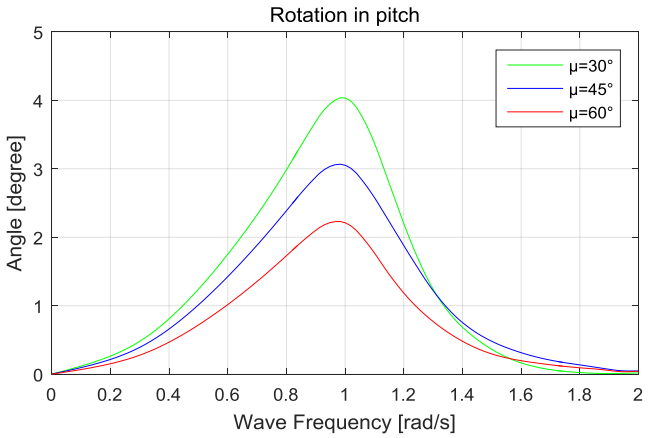

(c) Pitch angle

Figure 2.15: Displacement of the single island

From the above figures, one can see that the heave displacement is 1 in very low frequency, which equals to the wave amplitude in this case, so the heave motion of the island will follow the surface elevation in a very long wave. Also, the heave damping is critical in determining their response amplitudes (Fan et al., 2010), which

can be seen in the reduction of heave response amplitude. A similar result for the heave motion of a craft is discussed by Bandas and Falzarano (2011). Generally, the peak in motion response amplitude is caused by excitation of natural frequency in corresponding mode and the motion amplitudes peak at resonance frequency as motions parallel to wave direction. For this case, the roll motion appears to have a significant response for 3.8 degree at the frequency of 1 rad/s when the angle of attack is $60°$ and the pitch motion appears to have a significant response for 4 degrees at the frequency of 1 rad/s when the angle of attack is $30°$, which are all satisfied the small angle assumption in the linear theory. Besides, one should note that the motion response depends on the added mass, damping and stiffness matrices of the island while the force response only depends on the wave excitations.

Chapter 3

Two-island model

In this chapter, a two-island is being analyzed on the basis of the last chapter. The focus is the hydrodynamic effect and hydrodynamic interactions between the two floating islands of the identical shapes. Also, the connecting method for the two islands will be designed. The goal of this chapter is to learn the motions of the floating islands under the effect of waves and hydrodynamic interactions. What calls for special attention is that all the assumptions for the single island are still hold

3.1 The design of the islands

3.1.1 Dimension parameters

Two identical equilateral triangles and the connecting springs constituted the two islands model. A second island with the same geometry and inertia properties is implemented at a horizontal distance of 4 meters to the first island. Also, each floating island has six degrees of freedom respectively, twelve degrees of freedom in the system.

In this case, the origin is still settled at a fixed point that is on the mean water surface but not aligned to the center of gravity of triangle that was set for the single island. The origin lies at the midpoint of the line between the two centers of gravity that is shown in figure 3.1. The horizontal distance between the two islands is 4 meters, which is named ‘gap' in this case. The left one was named triangle 1, and the right one was named triangle 2. The two islands model coordinates defined in the earth-fixed coordinate frame can be denoted by:

$$x_i = [x_1 \quad y_1 \quad z_1 \quad \phi_1 \quad \theta_1 \quad \psi_1 \quad x_2 \quad y_2 \quad z_2 \quad \phi_2 \quad \theta_2 \quad \psi_2]^T \qquad (3.1)$$

In which, $\mathrm{x}, \mathrm{y}, \mathrm{z}$ represent surge, sway, heave displacement respectively, ϕ, θ and ψ represent roll, pitch and yaw angle respectively. The subscripts 1 and 2 designate the triangle 1 and 2 separately. However, one of the assumptions in this thesis is the bottom plane is the only plane will be considered. Thus, only heave, roll and pitch motions exist, and the displacement matrix can be reduced as:

$$x_i = [\, z_1 \quad \phi_1 \quad \theta_1 \quad z_2 \quad \phi_2 \quad \theta_2]^T \qquad (3.2)$$

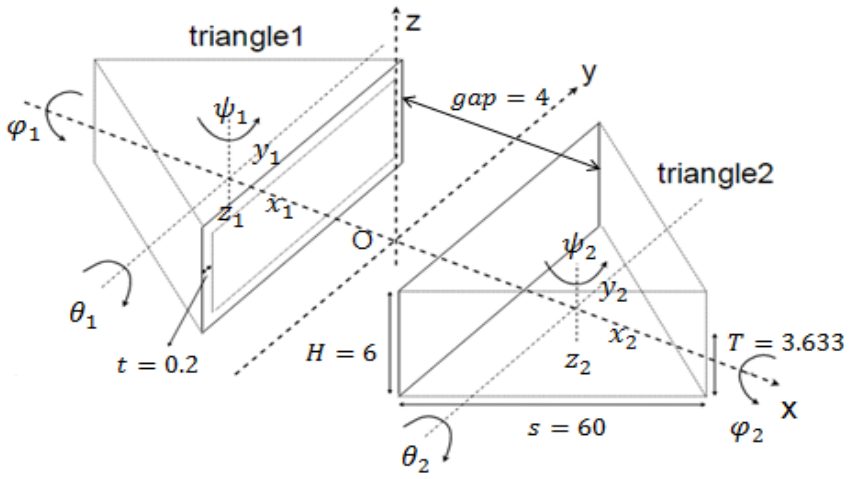

Figure 3.1: The two islands model

Similarly, the floating island will be built in the North Sea and the water depth is 50 meters in this case. Again, all the parameters are described in figure 3.1 and table 3.1. Note that two triangles have the selfsame dimensions, which is also precisely the same as the design of the single island.

Table 3.1 The dimensions of triangle 1 (the same as triangle 2)

side length(m)	side height (m)	wall thickness (m)	steel density (kg/m^3)	draft(m)	mass (kg)	gap(m)
60	6	0.2	7850	3.633	5805421	4

3.1.2 Mooring configuration

In this case, the mooring lines are still considered as linear spring as we assumed for the single island model. Three identical translational springs of stiffness k_0 are installed at the three midpoints of corners of triangle 1 separately to provide the normal restoring force in the x-y plane, the other ends of spring are connected to three fixed-point respectively. Also, a rotational spring of stiffness k_r is set up at the center of the triangle to restrain the rotation of triangle in the x-y plane that is fastened to a monopile that does not affect the motions of the structure. The mooring configuration for triangle 2 is the same as that for triangle 1.

In particular, the connecting method for the two islands is the exclusive mooring system when compared with that in the single island model. Four translational springs and two shear springs constitute the connecting springs' system, which provides the restoring forces and moments to keep the stability of relative position.

The mooring configuration for the two islands model is shown in figure 3.2. Also, some parameters are shown in table 3.2.

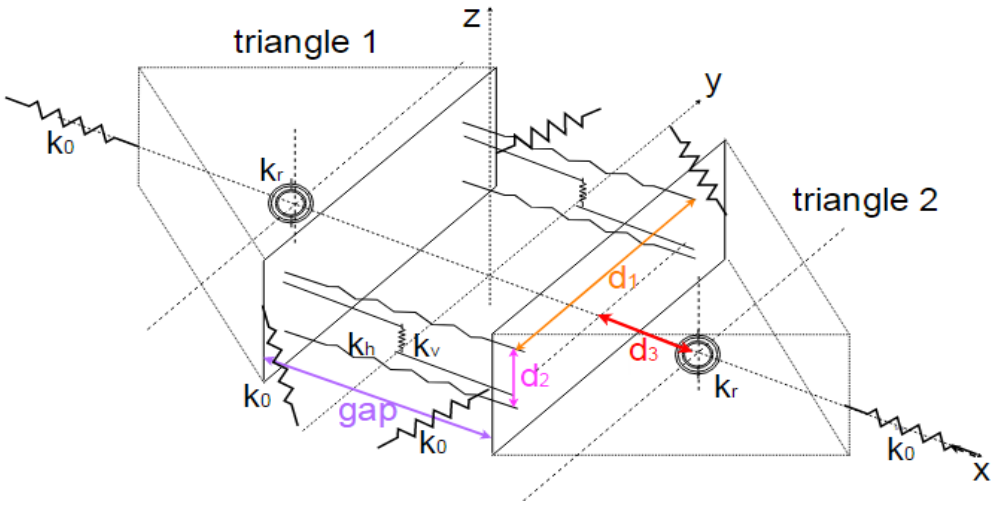

Figure 3.2: Mooring configuration for the two islands model

Table 3.2 Parameters that are used in the mooring system for the two islands model

k_0 (N/m)	k_r (Nm)	k_h (N/m)	k_v (N/m)	d_1 (m)	d_2 (m)	d_3 (m)	gap(m)
$1 \cdot 10^7$	$1 \cdot 10^9$	$1.5 \cdot 10^5$	$1.5 \cdot 10^5$	50	4	17.32	4

This mooring configuration convenient to manufacture, implement and disconnect. The stiffness coefficients $\mathrm{k_0}$, $\mathrm{k_r}$, k_0 and k_r are determined by the limiting displacements and optimal practical selections.

3.2 Equations of motion

In this section, a structural model is designed for prediction of the movements and loading of the two floating islands model. The primary method is the same as we used for the single island model. The potential theory and the Lagrangian equations are used again. Note that all the linear assumptions still hold.

3.2.1 Lagrange equation

As described in the last chapter, the Lagrange equation whose function is similar to Newton's second law is a good way to describe the motions of these two islands model. The standard Lagrange function L is defined as:

$$L = T - V \tag{3.3}$$

Where T and V are the total kinetic and corresponding potential energies respectively. The total kinetic energy is:

$$T = \frac{1}{2}\sum_{i,j=1}^{12} m_{ij}\,\dot{x}_i\dot{x}_j + \frac{1}{2}\sum_{i,j=1}^{12} a_{ij}\,\dot{x}_i\dot{x}_j \tag{3.4}$$

The generic Euler-Lagrange equation is then obtained by:

$$\frac{d}{dt}\left(\frac{\partial L}{\partial \dot{x}_\iota}\right)+\frac{\partial D}{\partial \dot{x}_\iota}-\frac{\partial L}{\partial x_i}=Q_i \tag{3.5}$$

Where D is the damping force:

$$D=\frac{1}{2}\sum_{i,j=1}^{12} b_{ij}\,\dot{x}_\iota \dot{x}_J \tag{3.6}$$

All the parameters are defined the same as described in equation 2.10. The only difference is there are 12 degrees of freedom for the two island model. Again, each part of the Lagrange equation will be solved separately in the following sections.

3.2.2 Mass

The mass matrix for these two islands model can be easily obtained from the single island case. The only difference is three modes for two islands should be considered:

$$\boldsymbol{M}=\begin{bmatrix} m & 0 & 0 & 0 & 0 & 0 \\ 0 & J_4 & 0 & 0 & 0 & 0 \\ 0 & 0 & J_5 & 0 & 0 & 0 \\ 0 & 0 & 0 & m & 0 & 0 \\ 0 & 0 & 0 & 0 & J_{10} & 0 \\ 0 & 0 & 0 & 0 & 0 & J_{11} \end{bmatrix} \tag{3.7}$$

In which, 4,5 and 10,11 indicate the roll and pitch mode of triangle 1 and triangle 2 respectively, the moments of inertia can be calculated in the same way as described in the last chapter.

3.2.3 The assumptions for the hydrodynamic analysis

In this case, two assumptions for the hydrodynamic analysis for the single island model are still held:

1. The bottom planes of two triangles are the only two surfaces that are considered in the study of motions. Thus the problem can be solved in six DOFs: heave, roll and pitch for two triangles.
2. The z-coordinate of the bottom plane is set as zero in the process of calculation for the hydrodynamic forces.

3.2.4 Added mass and damping coefficients

The basic principle for the generation of the added mass and radiation damping has been interpreted in the last chapter. However, a new issue, hydrodynamic interaction, appears when the hydrodynamic loads on one structure are influenced by the presence of the other structures, this interaction phenomenon can become more critical due to undesired relative motion response between two islands. Hydrodynamic interaction between two (or more) floating bodies can be considered

as scattering effect and resonance forces due to trapped waves (Durran, 2015) between the bodies, which are resonant oscillations whose amplitude and wavelength are considerably sensitive to variations in the structure of the flow impinging on the body. For the radiation force, one radiated island can play a role as a wave maker to the others. At frequencies of Helmholtz resonance (Hong et al., 2005) where fierce up and down motion of trapped water between two islands occurs, the huge jumps can be seen in the hydrodynamic forces curves.

When we only considered the heave, roll and pitch for the bottom plane, the added mass and damping matrixes for the two islands model are defined as follows:

$$\boldsymbol{A} = \begin{bmatrix} a_{33} & a_{34} & a_{35} & a_{39} & a_{3,10} & a_{3,11} \\ a_{43} & a_{44} & a_{45} & a_{49} & a_{4,10} & a_{4,11} \\ a_{53} & a_{54} & a_{55} & a_{59} & a_{5,10} & a_{5,11} \\ a_{93} & a_{94} & a_{95} & a_{99} & a_{9,10} & a_{9,11} \\ a_{10,3} & a_{10,4} & a_{10,5} & a_{10,9} & a_{10,10} & a_{10,11} \\ a_{11,3} & a_{11,4} & a_{11,5} & a_{11,9} & a_{11,10} & a_{11,11} \end{bmatrix}$$

$$\boldsymbol{B} = \begin{bmatrix} b_{33} & b_{34} & b_{35} & b_{39} & b_{3,10} & b_{3,11} \\ b_{43} & b_{44} & b_{45} & b_{49} & b_{4,10} & b_{4,11} \\ b_{53} & b_{54} & b_{55} & b_{59} & b_{5,10} & b_{5,11} \\ b_{93} & b_{94} & b_{95} & b_{99} & b_{9,10} & b_{9,11} \\ b_{10,3} & b_{10,4} & b_{10,5} & b_{10,9} & b_{10,10} & b_{10,11} \\ b_{11,3} & b_{11,4} & b_{11,5} & b_{11,9} & b_{11,10} & b_{11,11} \end{bmatrix} \tag{3.8}$$

Similarly, the added mass and damping coefficients a_{kj} and b_{kj} can be expressed as follows:

$$a_{kj} = -Re\left[\rho \iint_{S_0} \phi_j \cdot n_k \cdot dS_0\right]$$

$$b_{kj} = -Im\left[\rho\omega \iint_{S_0} \phi_j \cdot n_k \cdot dS_0\right] \tag{3.9}$$

Note that there is a slightly difference compared with the previous chapter, the subscript $j = 3,4,5,9,10,11$ in this case

3.2.4.1 Boundary conditions for radiation potentials

All four boundary conditions for the radiation potentials that described in the last chapter must be satisfied in like manner for this case.

3.2.4.2 Solving the radiation potentials

The potentials can be solved in the same way as mentioned in the last chapter as follows:

$$\phi_j(x,y,z) = \frac{1}{4\pi}\iint_{S_0} \sigma_j(\hat{x},\hat{y},\hat{z}) \cdot G(x,y,z,\hat{x},\hat{y},\hat{z}) dS_0 \tag{3.10}$$

Where $j = 3,4,5,9,10,11$ in this case. Then the panel method is used again. Each triangle has been divided into 16 panels, thus there 32 identical triangular panels in total are used to solve the potentials, which is shown in figure 3.3. Again, each source point locates at the centroid of the panel and the coordinate of panel n is $(x_{pn}, y_{pn}, 0)$.

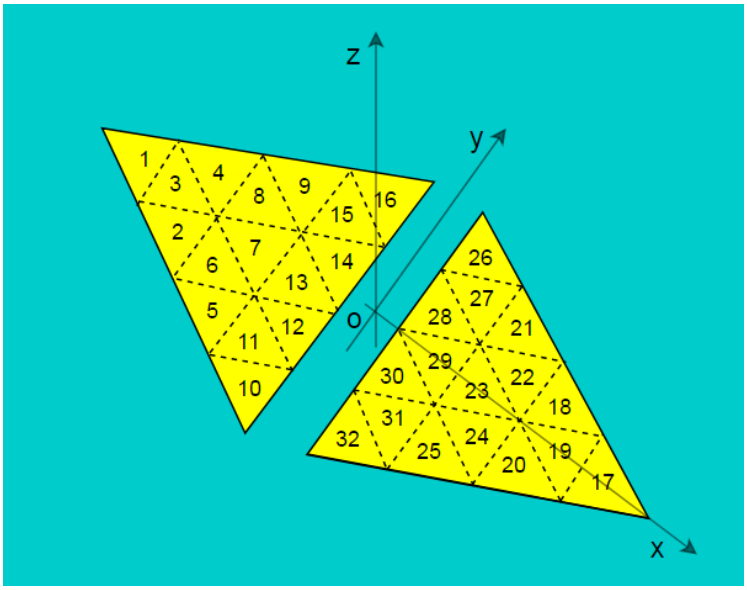

Figure 3.3: Panels for two floating islands

According to the boundary condition at the surface of the floating structure:

$$\frac{\partial \phi_j}{\partial n} = f_j$$

Substituting the potential function in the boundary condition:

$$-\frac{1}{2}\sigma_{mj} + \frac{1}{4\pi}\sum_{n=1}^{32} \sigma_{nj} \cdot \frac{\partial G_{mn}}{\partial n} \Delta S_n = f_{mj} \tag{3.11}$$

For the two islands model, there are 32 equations because the boundary condition must be satisfied with the collection points of all the 32panels. There are also 32 unknowns due to each panel has its own source strength. Hence, the system of equations for solving the source strength for the radiation potential becomes:

$$\begin{bmatrix} A_{11} & \cdots & A_{1,32} \\ \vdots & \ddots & \vdots \\ A_{32,1} & \cdots & A_{32,32} \end{bmatrix} \cdot \begin{bmatrix} \sigma_{1,j} \\ \vdots \\ \sigma_{32,j} \end{bmatrix} = \begin{bmatrix} (f_j)_1 \\ \vdots \\ (f_j)_{32} \end{bmatrix} \tag{3.12}$$

Where:

$j = 3,4,5,9,10,11 = the\ radiation\ potential\ that\ is\ considered$

$A_{nn} = -\frac{1}{2} = influence\ of\ \ source\ at\ panel\ n\ on\ \frac{\partial \phi_j}{\partial n}\ at\ its\ own\ collocation\ point,$

$(n = 1,2, \dots 32)$

$A_{mn} = \frac{1}{4\pi}\frac{\partial G_{mn}}{\partial n}\Delta S_n = influence\ of\ \ source\ at\ panel\ n\ on\ \frac{\partial \phi_j}{\partial n}\ at\ collection\ point\ m,$

$(m = 1,2, \dots 32)$

$\sigma_{n,j} = unknown\ source\ strength\ of\ radiation\ potential\ in\ j-th\ mode\ at\ panel\ n$

$\left(f_j\right)_m = local\ normal\ direction\ due\ to\ motion\ in\ direction\ j\ at\ panel\ n$

It should be noted that all the panels of two triangles should be considered as source when one calculating the source strength and the Green's function for one triangle, not only the radiating one. However, only the source points on the triangle itself should be accounted for the integral of potential. Then, the heave, roll and pitch radiation potentials for triangle 1 and 2 can be solved by:

For j=3,4,5:

$$\phi_{j,1}(x,y) = \sum_{n=1}^{16} \phi_{n,j}(x,y,z) = \sum_{n=1}^{16} \frac{1}{4\pi} \iint_{S_0} \sigma_{n,j}(\hat{x},\hat{y}) \cdot G(x,y,\hat{x},\hat{y}) d\hat{x} d\hat{y}$$

For j=9,10,11:

$$\phi_j{}'(x,y) = \sum_{n=17}^{32} \phi_{n,j}(x,y,z) = \sum_{n=17}^{32} \frac{1}{4\pi} \iint_{S_0} \sigma_{n,j}(\hat{x}',\hat{y}') \cdot G(x,y,\hat{x}',\hat{y}') d\hat{x}' d\hat{y}' \quad (3.13)$$

Where $(\hat{x},\hat{y})$ denotes the panel centroid coordinate of triangle 1 and $(\hat{x}',\hat{y}')$ denotes that of triangle 2. Substituting the results of radiation potentials at different frequencies in equation 3.17 to obtain the added mass and damping coefficients. Note that due to the zero terms from the results, the added mass and damping matrices can be rewritten as:

$$\boldsymbol{A} = \begin{bmatrix} a_{33} & 0 & a_{35} & a_{39} & 0 & a_{3,11} \\ 0 & a_{44} & 0 & 0 & a_{4,10} & 0 \\ a_{53} & 0 & a_{55} & a_{59} & 0 & a_{5,11} \\ a_{93} & 0 & a_{95} & a_{99} & 0 & a_{9,11} \\ 0 & a_{10,4} & 0 & 0 & a_{10,10} & 0 \\ a_{11,3} & 0 & a_{11,5} & a_{11,9} & 0 & a_{11,11} \end{bmatrix}$$

$$\boldsymbol{B} = \begin{bmatrix} b_{33} & 0 & b_{35} & b_{39} & 0 & b_{3,11} \\ 0 & b_{44} & 0 & 0 & b_{4,10} & 0 \\ b_{53} & 0 & b_{55} & b_{59} & 0 & b_{5,11} \\ b_{93} & 0 & b_{95} & b_{99} & 0 & b_{9,11} \\ 0 & b_{10,4} & 0 & 0 & b_{10,10} & 0 \\ b_{11,3} & 0 & b_{11,5} & b_{11,9} & 0 & b_{11,11} \end{bmatrix} \quad (3.14)$$

The added mass and damping coefficients for heave, roll and pitch are shown in figure 3.4 and 3.5 separately as a function of frequency. The remaining added mass and damping coefficients are shown in Appendix B and C respectively.

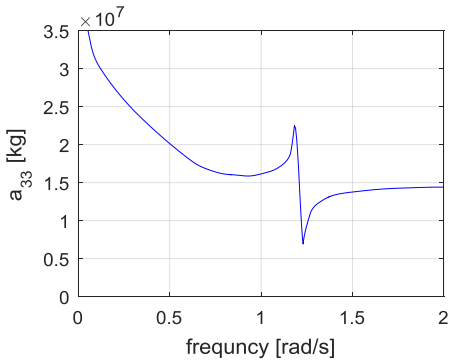

(a) a_{33}

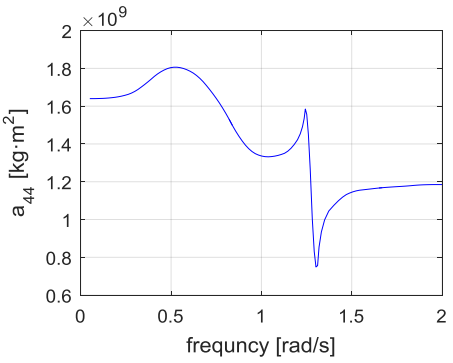

(b) a_{44}

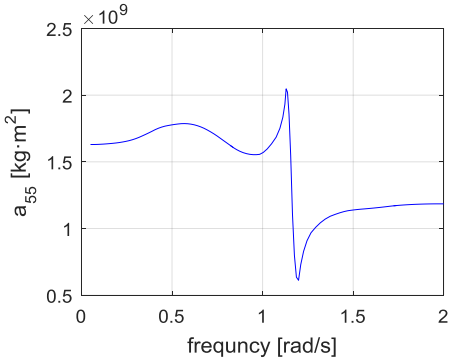

(c) a_{55}

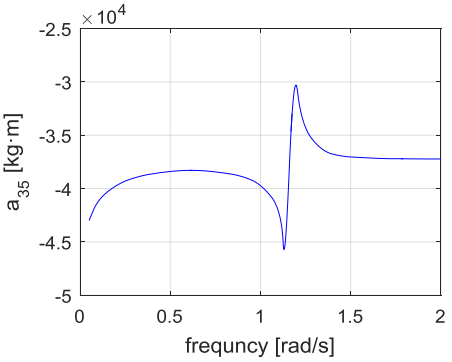

(d) a_{35}

Figure 3.4: Added mass for heave, roll and pitch

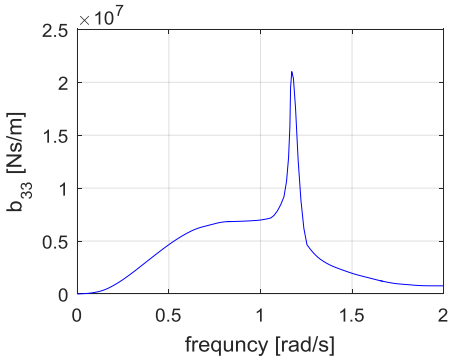

(a) b_{33}

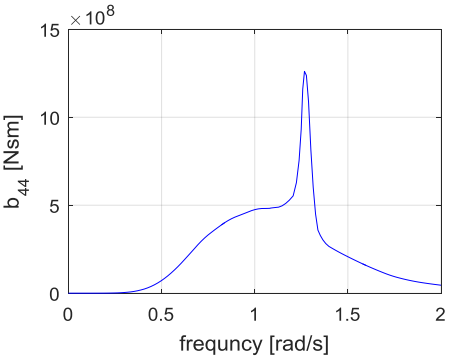

(b) b_{44}

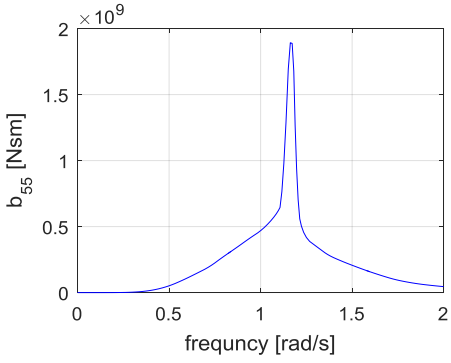

(c) b_{55}

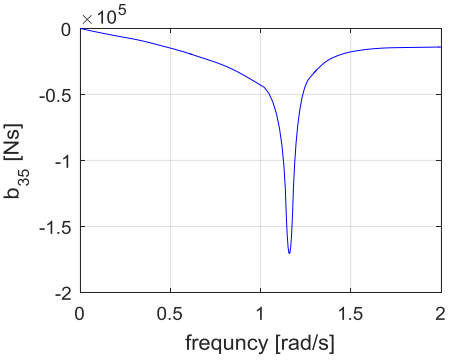

(d) b_{35}

Figure 3.5: Damping coefficients for heave, roll and pitch

From above figures, it can be obviously observed that the huge jumps in the curves of added mass and the spikes in the curves of damping, which are owing to the hydrodynamic interaction appears around 1.16 rad/s due to the resonance of trapped wave between two islands. Besides that hydrodynamic interaction, all the added mass and damping coefficient curves have a similar variation trend as that for the single island.

3.2.5 Wave excitation

Similarly, the wave exciting force of the two floating islands in regular waves can be split up into two parts: the Froude–Krylov force and the diffraction force. Compared with the wave excitation in the single island, the Froude-Krylov force has not changed at all. However, the diffraction problem is considerably different from that in the single island due to the hydrodynamic interaction. In diffraction analysis for the two islands, the island in the weather side acts as breakwater while the island in the lee side acts as a quay (Hong et al., 2005). At frequencies of Helmholtz, the exciting forces curves reach the peak.

3.2.5.1 Froude–Krylov force

As previously mentioned, the Froude–Krylov force is a hydrodynamical force formed by the undisturbed wave, assuming the water is not affected by the presence of the object. Hence the Froude–Krylov force for one island will not be influenced by the presence of the added one.

Homogeneously, the Froude–Krylov forces and moments can be calculated as follows:

$$\vec{\mathrm{F}}_{\mathrm{FK}} = -\iint_{\mathrm{S}_0} (\mathrm{p}_0 \cdot \vec{\mathrm{n}}) \mathrm{dS}_0 \tag{3.15}$$

$$\vec{M}_{FK} = -\iint_{S_0} p_0 \cdot (\vec{r} \times \vec{n}) dS_0 \tag{3.16}$$

Where:
S_0 = The area of the wetted surface $[\mathrm{m}^2]$
$\vec{r}$ = The location vector that is the three-component position vector indicating the x, y and z coordinate at the shell of the floating island.
$\vec{n}$ = The body's normal vector pointing into the water that is the three-component normal vector of unit length.

The results of the Froude–Krylov forces of triangle 1 and triangle 2 against the frequencies with the angles of attack equal to $30°$, $45°$ and $60°$ are shown in figure 3.6 respectively.

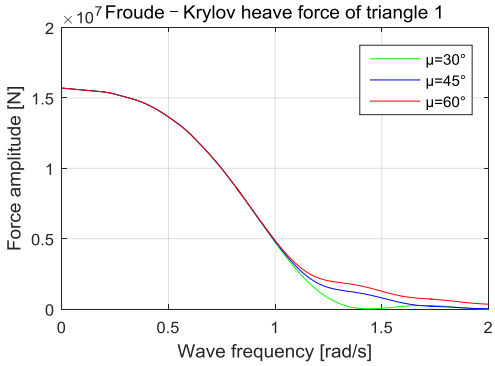

(a) Froude–Krylov heave force of triangle 1

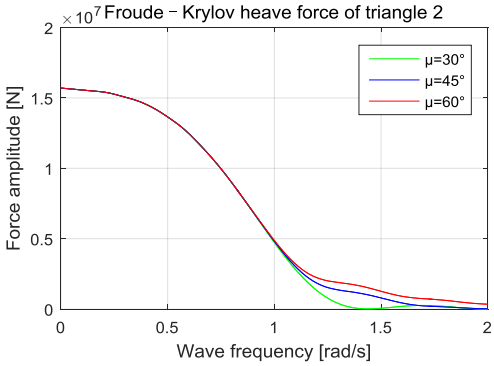

(b) Froude–Krylov heave force of triangle 2

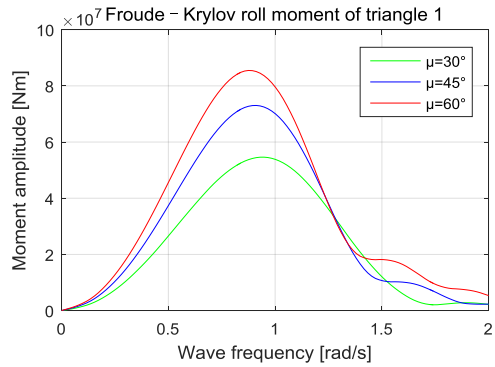

(c) Froude–Krylov roll moment of triangle 1

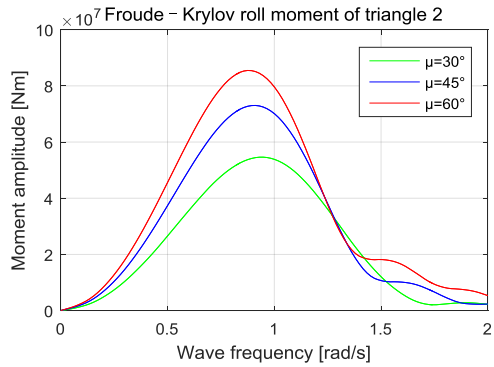

(d) Froude–Krylov roll moment of triangle 2

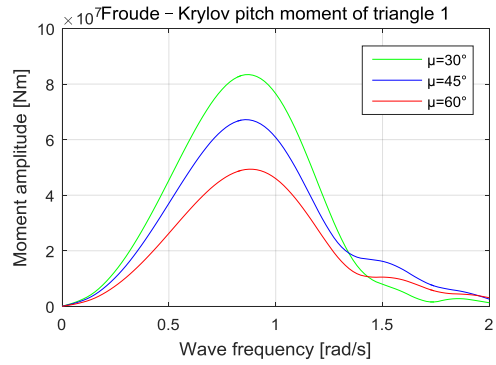

(e) Froude–Krylov pitch moment of triangle 1

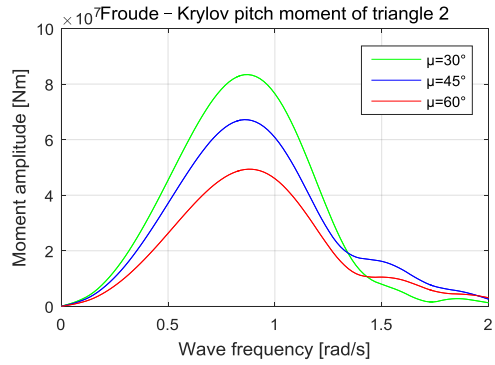

(f) Froude–Krylov pitch moment of triangle 2

Figure 3.6: Froude–Krylov forces in three modes of triangle 1 and 2

As can be seen from the above figures, the Froude–Krylov forces keep the same outlines when compared with that in the single island model. It is easy to interpret that the multibody presence will not influence the undisturbed wave due to we assume the undisturbed wave would penetrate right through the body. Thus, the Froude–Krylov forces for the two models are the same.

3.2.5.2 Boundary conditions for diffraction potential

All the boundary conditions for the diffraction potential that described in the last chapter must be satisfied in like manner for this case.

3.2.5.3 Solving the diffraction potential

The approach to solving the diffraction potential for the two islands model is similar to the method that was used for the single island model. The only change is both two triangles have 16 panels like the situation for solving the radiation potentials in this chapter. The interface condition is:

$$\frac{\partial \phi_0}{\partial n} + \frac{\partial \phi_7}{\partial n} = 0$$

$$-\frac{1}{2}\sigma_{mj} + \frac{1}{4\pi}\sum_{n=1}^{32} \sigma_{n,7} \cdot \frac{\partial G_{mn}}{\partial n} \Delta S_n = -\left(\frac{\partial \phi_0}{\partial n}\right)_m \tag{3.17}$$

The system of equations for solving the source strength for the diffraction potential becomes:

$$\begin{bmatrix} A_{11} & \cdots & A_{1,32} \\ \vdots & \ddots & \vdots \\ A_{32,1} & \cdots & A_{32,32} \end{bmatrix} \cdot \begin{bmatrix} \sigma_{1,7} \\ \vdots \\ \sigma_{32,7} \end{bmatrix} = \begin{bmatrix} -\left(\frac{\partial \phi_0}{\partial n}\right)_1 \\ \vdots \\ -\left(\frac{\partial \phi_0}{\partial n}\right)_{32} \end{bmatrix} \tag{3.18}$$

Where:

$A_{nn} = -\frac{1}{2} = influence\ of\ \ source\ at\ panel\ n\ on\ \frac{\partial \phi_7}{\partial n}\ at\ its\ own\ collocation\ point,$
$(n = 1,2, \dots 32)$

$A_{mn} = \frac{1}{4\pi}\frac{\partial G_{mn}}{\partial n}\Delta S_n = influence\ of\ \ source\ at\ panel\ n\ on\ \frac{\partial \phi_7}{\partial n}\ at\ collection\ point\ m,$
$(m = 1,2, \dots 32)$

$\sigma_{n,7} = unknown\ source\ strength\ of\ \ diffraction\ potential\ \ at\ panel\ n$

Similarly, solving the Green's function and then obtaining the diffraction potential function $\phi_7(x, y)$ for triangle 1 and the diffraction potential function $\phi_7{}'(x, y)$ for triangle 2:

$$\phi_7(x, y) = \sum_{n=1}^{16} \phi_{n,7}(x, y, z) = \sum_{n=1}^{16} \frac{1}{4\pi} \iint_{S_0} \sigma_{n,7}(\hat{x}, \hat{y}) \cdot G(x, y, \hat{x}, \hat{y}) d\hat{x} d\hat{y}$$

$$\phi_7{}'(x, y) = \sum_{n=17}^{32} \phi_{n,7}(x, y, z) = \sum_{n=17}^{32} \frac{1}{4\pi} \iint_{S_0} \sigma_{n,7}(\hat{x}', \hat{y}') \cdot G\left(x, y, \hat{x}', \widehat{y'}\right) d\hat{x}' d\hat{y}' \tag{3.19}$$

Substituting the results of diffraction potential at different frequencies in the following equation to obtain the diffraction forces:

$$p_7 = \rho \frac{\partial \Phi_7}{\partial \mathrm{t}}$$

$$\vec{F}_D = -\iint_{S_0} (p_7 \cdot \vec{n}) dS_0$$

$$\vec{M}_D = -\iint_{S_0} p_7 \cdot (\vec{r} \times \vec{n}) dS_0 \qquad (3.20)$$

Where $\vec{r} = (x - x_c, y - y_c, z - z_c)$ is the coordinate of the considered location of the shell of the structure in the body-fixed axes system, the coordinate of the center of gravity of the structure is (x_c, y_c, z_c) . The results of the diffraction forces at various frequencies with the angle of attack equal to $30°$ $45°$ and $60°$ are shown in figure 2.10.

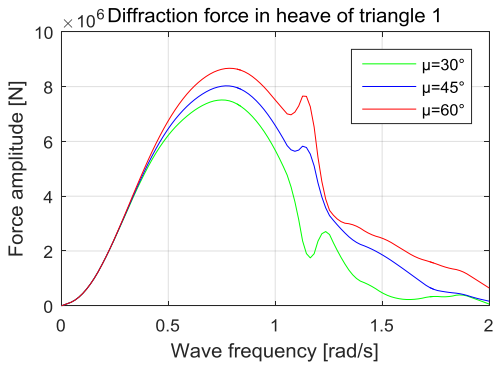

(a) Diffraction heave force of triangle 1

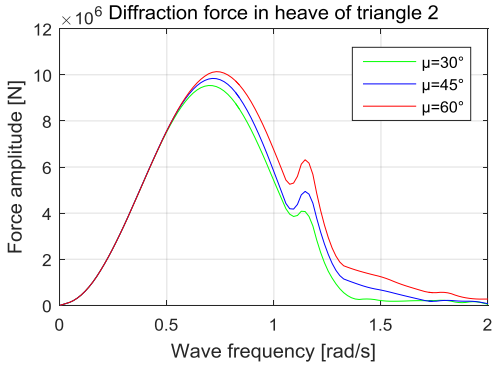

(b) Diffraction heave force of triangle 2

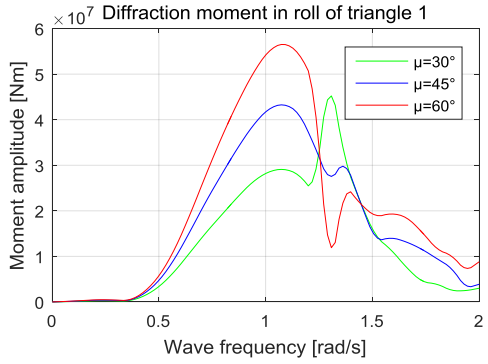

(c) Diffraction roll moment of triangle 1

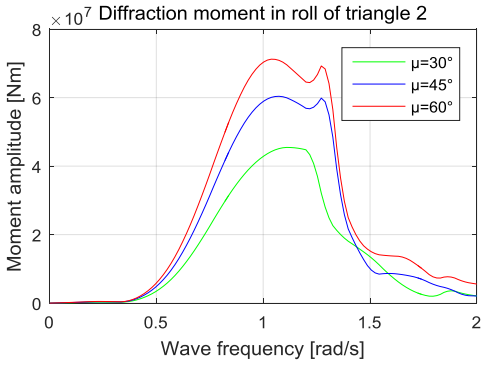

(d) Diffraction roll moment of triangle 2

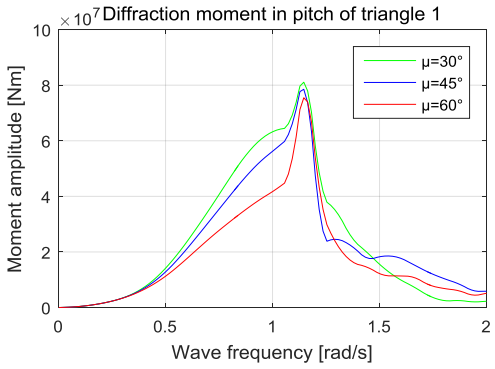

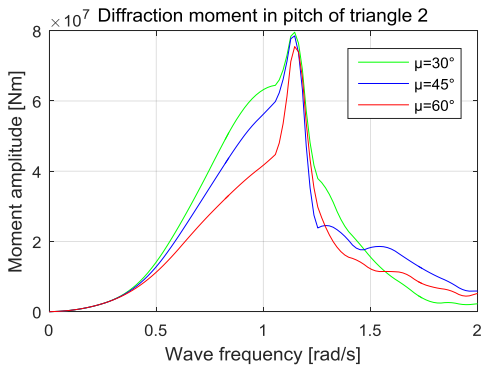

(e) Diffraction pitch moment of triangle 1 (f) Diffraction pitch moment of triangle2

Figure 3.7: Diffraction forces in three modes of triangle 1 and 2

From figure 3.7, one can see that there is a prominent peak at the frequency = 1.16 rad/s in heave mode, a peak at the frequency = 1.37 rad/s in roll mode and a peak at the frequency = 1.2 rad/s in pitch mode for triangle 1 due to hydrodynamic interaction in diffraction forces. This phenomenon occurs on the curves for triangle 2 as well.

3.2.5.4 Total wave exciting forces

Now, the expressions for the Froude–Krylov forces and diffraction forces for the two islands model are obtained. The total wave exciting force can be expressed as the summation of these two parts:

$$F_{wave} = F_{FK} + F_D \tag{2.76}$$

The total wave exciting forces at various frequencies in heave, pitch and roll motion with the angle of attack equals to $30°$ $45°$ and $60°$ are shown in figure 2.11.

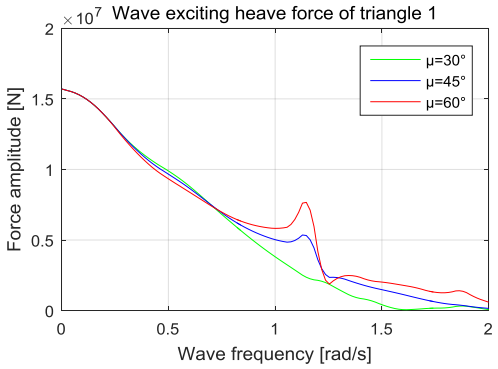

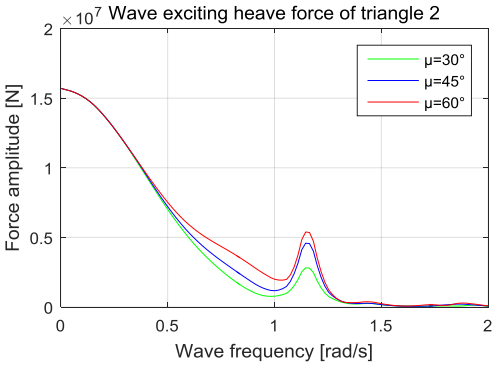

(a) Wave exciting force in heave of triangle 1

(b) Wave exciting force in heave of triangle 2

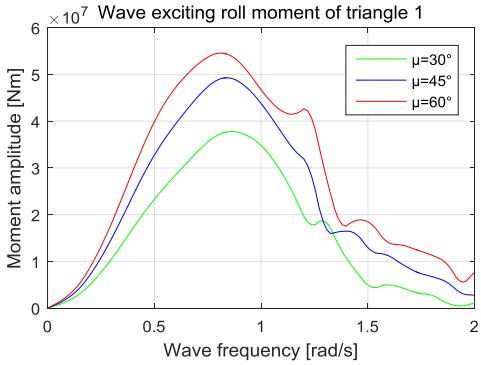

(c) Wave exciting moment in roll of triangle 1

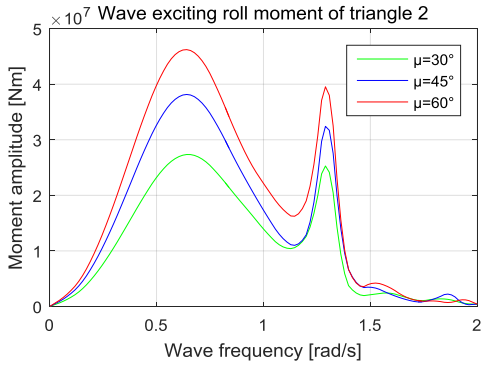

(d) Wave exciting moment in roll of triangle 2

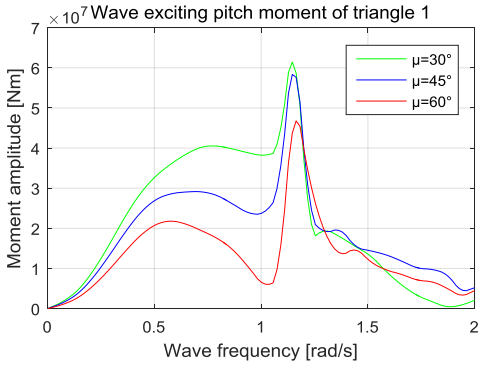

(e) Wave exciting moment in pitch of triangle 1

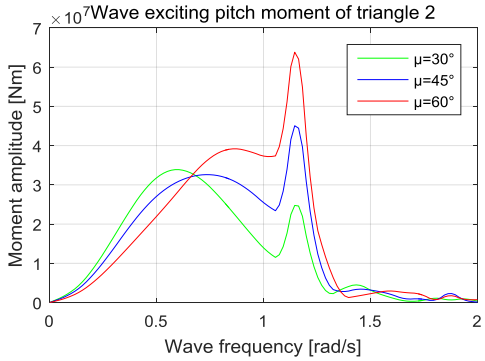

(f) Wave exciting moment in pitch of triangle 2

Figure 3.8: Total wave exciting forces in three modes of triangle 1 and 2

From the figures of wave exciting forces, it can be observed that there are three distinct peaks at frequency=1.16 rad/s, 1.37 rad/s and 1.2 rad/s on the curves for three modes of triangle 1 due to the hydrodynamic interaction, which did not appear in the single island. This peak may make the islands move more violently and increase the potential safety hazard. This phenomenon occurs on the curves for triangle 2 as well.

3.2.6 Stiffness

As mentioned in the last chapter, stiffness stands for the restoring force required to produce a unit displacement. In this chapter, besides the hydrostatic effect, mooring force and gravity that described in the last chapter, the connecting springs' effect must be considered as well.

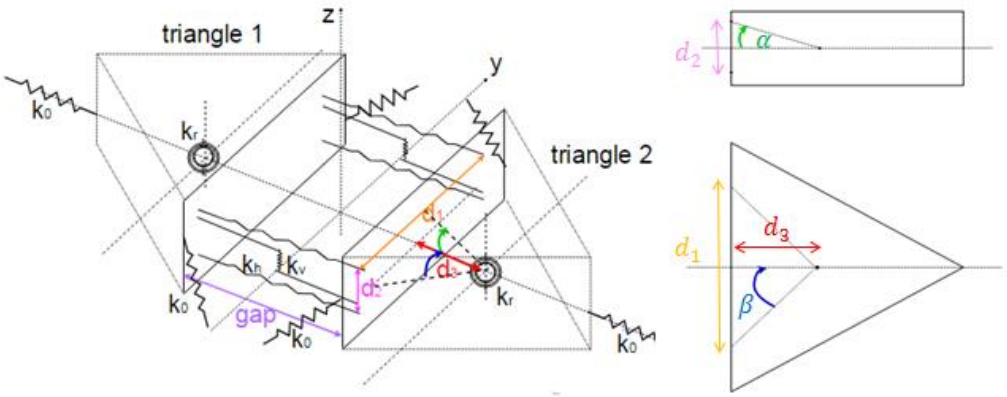

Figure 3.8 Specific mooring configuration

Firstly, the hydrostatic stiffness matrix could be found as follows when we only considered the heave, roll and pitch motions:

$$\boldsymbol{K}_{hydrostatic} = \begin{bmatrix} k_{33} & 0 & 0 & 0 & 0 & 0 \\ 0 & k_{44} & 0 & 0 & 0 & 0 \\ 0 & 0 & k_{55} & 0 & 0 & 0 \\ 0 & 0 & 0 & k_{99} & 0 & 0 \\ 0 & 0 & 0 & 0 & k_{10,10} & 0 \\ 0 & 0 & 0 & 0 & 0 & k_{11,11} \end{bmatrix} \tag{3.21}$$

Again, k_{ij} denotes the restoring force in i-direction due to the motion in j-direction. The hydrostatic coefficients for triangle 1 are identical to that for triangle 2, which means:

$$k_{33} = k_{99} \qquad k_{44} = k_{10,10} \qquad k_{55} = k_{11,11} \tag{3.22}$$

Besides, each value in the hydrostatic stiffness matrix remains the identical results in the last chapter due to the triangles are the same.

Equally, the potential energy due to hydrostatic effect can be found as:

$$V_{hs3} = \frac{1}{2}k_{33}{z_1}^2 \qquad V_{hs4} = \frac{1}{2}k_{44}{\varphi_1}^2 \qquad V_{hs5} = \frac{1}{2}k_{55}{\theta_1}^2$$

$$V_{hs9} = \frac{1}{2}k_{99}{z_2}^2 \qquad V_{hs10} = \frac{1}{2}k_{10,10}{\varphi_2}^2 \qquad V_{hs11} = \frac{1}{2}k_{11,11}{\theta_2}^2 \tag{3.23}$$

The potential energy due to gravity:

$$V_g = mgz_1 + mgz_2 \tag{3.24}$$

Based on the configuration of mooring lines (see figure 3.8), the potential energy due to mooring springs:

$$V_{m1} = \frac{1}{2}k_0[x_1 + \frac{\sqrt{3}s}{3}(1-\cos\theta_1) + \frac{\sqrt{3}s}{3}(1-\cos\psi_1)]^2$$

$$V_{m2} = \frac{1}{2}k_0(-x_1\cos 60° - y_1\cos 30° + \frac{s}{2}(1-\cos\varphi_1)\cos 30° + \frac{\sqrt{3}s}{6}(1-\cos\theta_1)\cos 60° + \frac{\sqrt{3}s}{3}(1 - \cos\psi_1))^2$$

$$V_{m3} = \frac{1}{2}k_0(-x_1\cos 60° + y_1\cos 30° + \frac{s}{2}(1-\cos\varphi_1)\cos 30° + \frac{\sqrt{3}s}{6}(1-\cos\theta_1)\cos 60° + \frac{\sqrt{3}s}{3}(1 - \cos\psi_1))^2$$

$$V_{m4} = \frac{1}{2}k_r{\psi_1}^2$$

$$V_{m5} = \frac{1}{2}k_0[-x_2 + \frac{\sqrt{3}s}{3}(1-\cos\theta_2) + \frac{\sqrt{3}s}{3}(1-\cos\psi_2)]^2$$

$$Vm_6 = \frac{1}{2}k_0(x_2\cos 60° - y_2\cos 30° + \frac{s}{2}(1-\cos\varphi_2)\cos 30° + \frac{\sqrt{3}s}{6}(1-\cos\theta_2)\cos 60° + \frac{\sqrt{3}s}{3}(1-\cos\psi_2))^2$$

$$V_{m7} = \frac{1}{2}k_0(x_2\cos 60° + y_2\cos 30° + \frac{s}{2}(1-\cos\varphi_2)\cos 30° + \frac{\sqrt{3}s}{6}(1-\cos\theta_2)\cos 60° + \frac{\sqrt{3}s}{3}(1-\cos\psi_2))^2$$

$$V_{m8} = \frac{1}{2}k_r{\psi_2}^2 \tag{3.25}$$

Based on the configuration of connecting springs (see figure 3.8), the potential energy due to connecting springs:

$$V_{c1} = \frac{1}{2}k_h[-x_1+x_2 - \left(\sqrt{{d_3}^2 + \left(\frac{d_2}{2}\right)^2}\cdot\cos(90°-\alpha-\theta_1) - d_3\right) + \left(d_3 - \sqrt{{d_3}^2 + \left(\frac{d_2}{2}\right)^2}\cdot\sin(\alpha-\theta_2)\right) + \left(d_3 - \sqrt{{d_3}^2 + \left(\frac{d_1}{2}\right)^2}\cdot\sin(90°-\beta-\psi_1)\right) - \left(\sqrt{{d_3}^2 + \left(\frac{d_1}{2}\right)^2}\cdot\cos(\beta-\psi_2) - d_3\right)]^2$$

$$V_{c2} = \frac{1}{2}k_h[-x_1+x_2 + \left(d_3 - \sqrt{{d_3}^2 + \left(\frac{d_2}{2}\right)^2}\cdot\sin(\alpha-\theta_1)\right) - \left(\sqrt{{d_3}^2 + \left(\frac{d_2}{2}\right)^2}\cdot\cos(90°-\alpha-\theta_2) - d_3\right) + \left(d_3 - \sqrt{{d_3}^2 + \left(\frac{d_1}{2}\right)^2}\cdot\sin(90°-\beta-\psi_1)\right) - \left(\sqrt{{d_3}^2 + \left(\frac{d_1}{2}\right)^2}\cdot\cos(\beta-\psi_2) - d_3\right)]^2$$

$$V_{c3} = \frac{1}{2}k_h[-x_1+x_2 - \left(\sqrt{{d_3}^2 + \left(\frac{d_2}{2}\right)^2}\cdot\cos(90°-\alpha-\theta_1) - d_3\right) + \left(d_3 - \sqrt{{d_3}^2 + \left(\frac{d_2}{2}\right)^2}\cdot\sin(\alpha-\theta_2)\right) - \left(\sqrt{{d_3}^2 + \left(\frac{d_1}{2}\right)^2}\cdot\cos(\beta-\psi_1) - d_3\right) + \left(d_3 - \sqrt{{d_3}^2 + \left(\frac{d_1}{2}\right)^2}\cdot\sin(90°-\beta-\psi_2)\right)]^2$$

$$V_{c4} = \frac{1}{2}k_h[-x_1+x_2 + \left(d_3 - \sqrt{{d_3}^2 + \left(\frac{d_2}{2}\right)^2}\cdot\sin(\alpha-\theta_1)\right) - \left(\sqrt{{d_3}^2 + \left(\frac{d_2}{2}\right)^2}\cdot\cos(90°-\alpha-\theta_2) - d_3\right) - \left(\sqrt{{d_3}^2 + \left(\frac{d_1}{2}\right)^2}\cdot\cos(\beta-\psi_1) - d_3\right) + \left(d_3 - \sqrt{{d_3}^2 + \left(\frac{d_1}{2}\right)^2}\cdot\sin(90°-\beta-\psi_2)\right)]^2$$

$$V_{c5} = \frac{1}{2}k_v[z_1 - z_2 + \frac{d_1}{2}\sin\varphi_1 - \frac{d_1}{2}\sin\varphi_2 - \left(d_3 + \frac{gap}{2}\right)\sin\theta_1 - \left(d_3 + \frac{gap}{2}\right)\sin\theta_2]^2$$

$$V_{c6} = \frac{1}{2}k_v\left[z_1 - z_2 - \frac{d_1}{2}\sin\varphi_1 + \frac{d_1}{2}\sin\varphi_2 - \left(d_3 + \frac{gap}{2}\right)\sin\theta_1 - \left(d_3 + \frac{gap}{2}\right)\sin\theta_2\right]^2 \tag{3.26}$$

Note that k_h and k_v represents the stiffness coefficient of the horizontal spring

and vertical spring respectively. Based on the multiply comparsion to find the proper values, it can be set as:

$$k_h = k_v = 0.01 * k_{33} \tag{3.27}$$

In summary, the total potential energy becomes:

$$V = V_{hs3} + V_{hs4} + V_{hs5} + V_{hs9} + V_{hs10} + V_{hs11} + V_g + V_{m1} + V_{m2} + V_{m3} + V_{m4} + V_{c1} + V_{c2} + V_{c3} + V_{c4} + V_{c5} + V_{c6} \tag{3.28}$$

3.3 Modelling results

Again, after substituting all above results of kinetic energies, potential energies and the generalized forces in the Euler-Lagrange equation, it can be rewritten as:

$$\frac{d}{dt}\left(\frac{\partial T}{\partial \dot{x}_i}\right) + \frac{\partial D}{\partial \dot{x}_i} - \frac{\partial V}{\partial x_i} = Q_i \tag{3.29}$$

Note that the small angle approximation in equation 3.85 is implemented after one solved the derivative of potential energy with respect to time. Then, the equations of motion for this six-DOF two floating islands system can be expressed as:

$$(\boldsymbol{M} + \boldsymbol{A})\ddot{\boldsymbol{x}} + \boldsymbol{B}\dot{\boldsymbol{x}} + \boldsymbol{K}\boldsymbol{x} = \boldsymbol{Q} \tag{3.30}$$

Where:

$$\boldsymbol{A} = \begin{bmatrix} a_{33} & 0 & a_{35} & a_{39} & 0 & a_{3,11} \\ 0 & a_{44} & 0 & 0 & a_{4,10} & 0 \\ a_{53} & 0 & a_{55} & a_{59} & 0 & a_{5,11} \\ a_{93} & 0 & a_{95} & a_{99} & 0 & a_{9,11} \\ 0 & a_{10,4} & 0 & 0 & a_{10,10} & 0 \\ a_{11,3} & 0 & a_{11,5} & a_{11,9} & 0 & a_{11,11} \end{bmatrix} \boldsymbol{B} = \begin{bmatrix} b_{33} & 0 & b_{35} & b_{39} & 0 & b_{3,11} \\ 0 & b_{44} & 0 & 0 & b_{4,10} & 0 \\ b_{53} & 0 & b_{55} & b_{59} & 0 & b_{5,11} \\ b_{93} & 0 & b_{95} & b_{99} & 0 & b_{9,11} \\ 0 & b_{10,4} & 0 & 0 & b_{10,10} & 0 \\ b_{11,3} & 0 & b_{11,5} & b_{11,9} & 0 & b_{11,11} \end{bmatrix}$$

$$\boldsymbol{K} = \begin{bmatrix} k_{33} + 2k_v & 0 & 38.64k_v & -2k_v & 0 & -38.64k_v \\ 0 & k_{44} + 1250k_v & 0 & 0 & -1250k_v & 0 \\ 38.64k_v & 0 & k_{55} + 16k_h + 746.52k_v & -38.64k_v & 0 & -16k_h - 746.52k_v \\ -2k_v & 0 & -38.64k_v & k_{33} + 2k_v & 0 & 38.64k_v \\ 0 & -1250k_v & 0 & 0 & k_{44} + 1250k_v & 0 \\ -38.64k_v & 0 & -16k_h - 746.52k_v & 38.64k_v & 0 & k55 + 16k_h + 746.52k_v \end{bmatrix}$$

$$\boldsymbol{M} = \begin{bmatrix} m & 0 & 0 & 0 & 0 & 0 \\ 0 & J_4 & 0 & 0 & 0 & 0 \\ 0 & 0 & J_5 & 0 & 0 & 0 \\ 0 & 0 & 0 & m & 0 & 0 \\ 0 & 0 & 0 & 0 & J_{10} & 0 \\ 0 & 0 & 0 & 0 & 0 & J_{11} \end{bmatrix} \quad \boldsymbol{Q} = \begin{bmatrix} F_{FK3} + F_{D3} \\ F_{FK4} + F_{D4} \\ F_{FK5} + F_{D5} \\ F_{FK9} + F_{D9} \\ F_{FK10} + F_{D10} \\ F_{FK11} + F_{D11} \end{bmatrix} \tag{3.31}$$

All the matrices have the same indications as described in last chapter. To see the effect of the connecting springs, the motions of triangle 1 and triangle 2 without connecting springs (scilicet two free floating islands) and the motions of triangle 1 and triangle 2 with connecting springs against the frequency with angles of attack equals to $30°$, $45°$ and $60°$ are shown in figure 3.15 and 3.16 respectively.

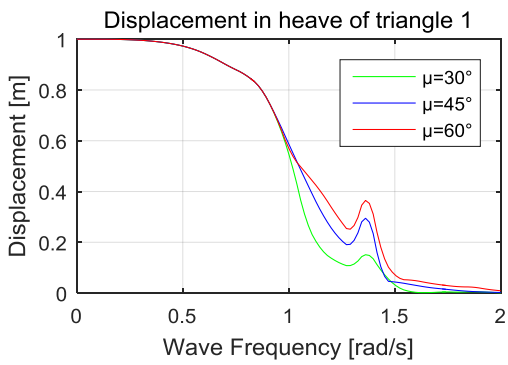

(a) Displacement of triangle 1 in heave without connecting springs

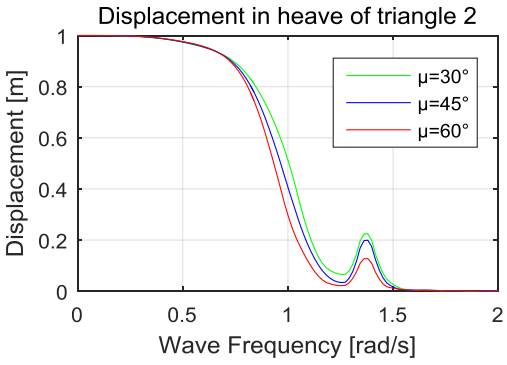

(a) Displacement of triangle 2 in heave without connecting springs

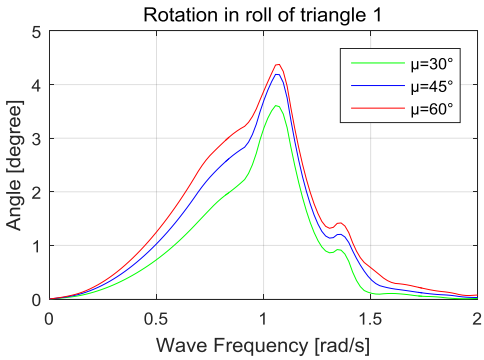

(c) Rotation of triangle 1 in roll without connecting springs

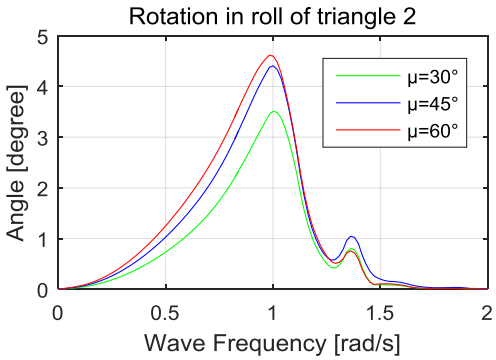

(d) Rotation of triangle 2 in roll without connecting springs

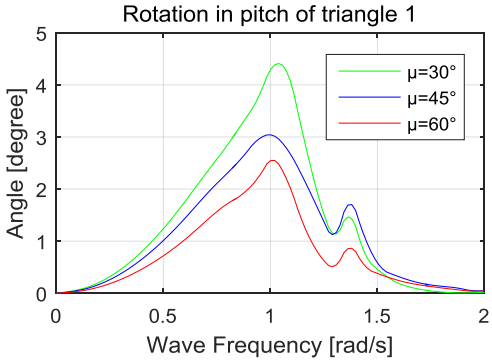

(e) Rotation of triangle 1 in pitch without connecting springs

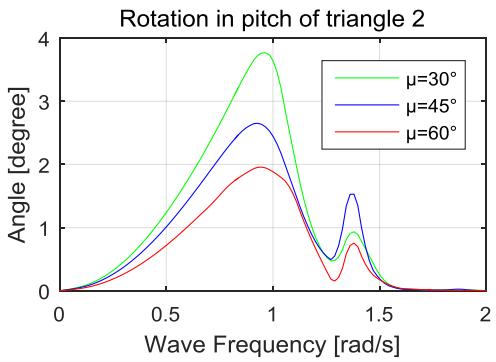

(f) Rotation of triangle 2 in pitch without connecting springs

Figure 3.15: Displacement of two free islands

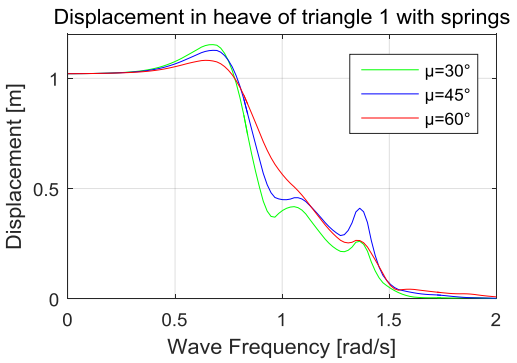

(a) Displacement of triangle 1 in heave with connecting springs

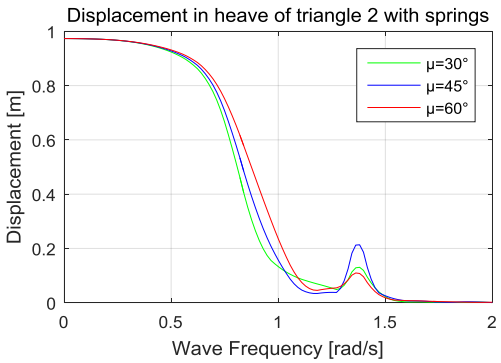

(b) Displacement of triangle 2 in heave with connecting springs

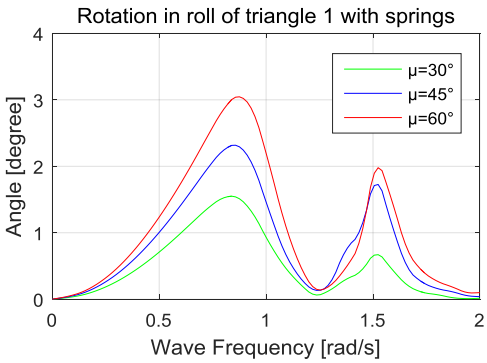

(c) Rotation of triangle 1 in roll with connecting springs

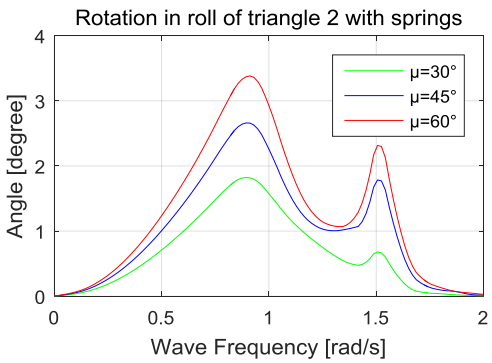

(d) Rotation of triangle 2 in roll with connecting springs

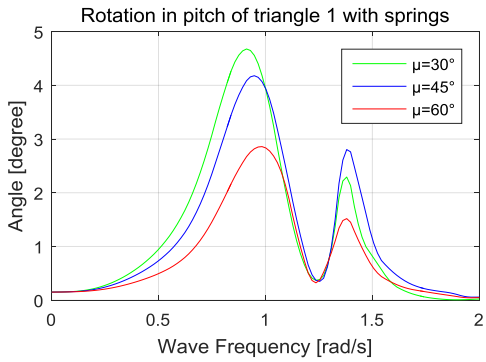

(e) Rotation of triangle 1 in pitch with connecting springs

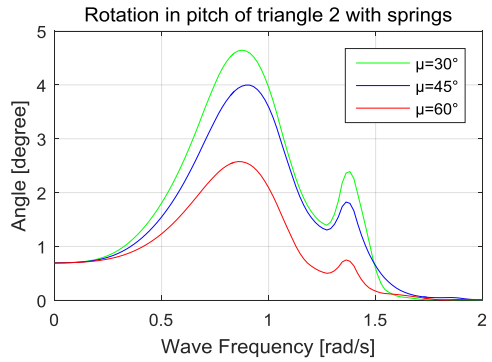

(f) Rotation of triangle 2 in pitch with connecting springs

Figure 3.16: Displacement of two constrained islands

From figure 3.15, one can see that motion responses are resulting from the combined effect of radiation and diffraction. Compared with the result for the single island in the last chapter, the most obvious difference is the peak due to the hydrodynamic interaction in each mode.

From figure 3.16, one can see that the apparent effect of the connecting springs. The roll motion of the constrained islands shows attenuated by 25% when compared with

the two free-floating islands. More than that, the peak responses in heave, roll and pitch due to the resonance are shifted to lower frequencies and almost out of the wave frequency range, hence reducing the possibility of resonant responses in those three modes.

Chapter 4

Summary and conclusions

4.1 Summary

In this thesis, two numerical models were analyzed in the frequency domain in the linear theory. The first part is the analysis for a single floating island model in regular waves and analyzed its dynamic frequency response functions. After the design of the island and the calculation for the hydrostatic effect, the panel method is used to solve the radiation and diffraction potential functions. Then, the added mass, damping and wave exciting forces are obtained. Finally, the motion responses are solved by using MATLAB ordinary differential equations solver (ode45). As can be seen from the results, the working conditions do not exceed the limiting conditions, which mean the design of the island is proper in assuming environmental conditions.

In the second part, a two islands model is built up on the basis of the single island model. The extra connecting springs are implemented to constrain the relative motion of two islands. The primary principle for the analysis of the two islands model is basically the same as the method used for the first model. A new problem appears for the second model is the hydrodynamic interactions effect, which widely exists in the multiple floating structures analysis. The ode45 solver is used again to address the motion response. As can be seen from the results of the second model, an obvious difference from the first model shows the influence of the hydrodynamic interaction. Also, a comparison between the two free islands and two constrained islands shows the effect of the connecting springs.

4.2 Conclusions

1. In the frequency domain simulation of the single island case, it can be observed that at the various angles of attack, the motions of the island might show the different response. Compared three angles of attack that are analyzed, for the roll motion, the highest response is $3.8°$, which appears at frequency = 1 rad/s with the angle of attack = $60°$. For the pitch motion, the highest response is $4°$, which appears at frequency = 1 rad/s with the angle of attack = $30°$. For the heave motion,

three angles of attack show similar trends. The highest responses are all equal to 1, which is the wave amplitude in this project. Based on this design, the pitch motion can be seen as the limiting condition. All the results satisfied the small angle assumption and in the reasonable range in the existing analysis, which proves the design of this single island is proper.

2. From the results of the two-island case, the hydrodynamic interaction has an obvious effect on the motion response when compared with that in the single island. The motions have peaks due to the hydrodynamic interaction. The Helmholtz response peak values are within acceptable limits. The strength of this hydrodynamic interaction is related to the angles of attack. Based on the analysis for three different angles of attack, the roll hydrodynamic interaction is most violent when the angle of attack is $60°$ while pitch hydrodynamic interaction is most violent when the angle of attack is $30°$.

3. The existence of connecting springs could significantly reduce the roll response by 25% a when compared to the two free islands. Moreover, the peak frequencies of three modes are shifted to lower frequencies and almost out of the wave frequency range, which reduce the probability of roll and pitch resonant responses, which is one of the initial goals for the flexible floating islands.

Bibliography

Callebaut, V. (2014). *Fertile cities, Vincent Callebaut architectures.* Liaoning Science and Technology Publishing House.

Ghassemi, H., and Yari, E. (2011). The Added Mass Coefficient computation of sphere, ellipsoid and marine propellers using Boundary Element Method. *Polish Maritime Research* 18(1), 17-26.

Koekoek, M. (2010). Connecting Modular Floating Structures: A General Survey and Structural Design of a Modular Floating Pavilion. Master's thesis. Delft University of Technology.

Das, S.N., and Das, S.K. (2004). Determination of coupled sway, roll, and yaw motions of a floating body in regular waves. *International Journal of Mathematics and* Mathematical Sciences 41(1), 2181-2197.

Veer, R.V. (2017). Floating Structures & Offshore Moorings. Lecture slides. Delft University of Technology.

Salvesen, N., Tuck, E.O., and Faltinsen, O.M. (1970). *Ship motions and sea loads*. Norske Veritas.

Myers, J.A. (1962). Handbook of equations for mass and area properties of various geometrical shapes. U.S. Naval Ordnance Test Station.

Wallis, G.B. (2011). Added mass. Retrieved July 19, 2018, from http://thermopedia.com/content/289/

Journée, J.M.J, and Massie, W.W. (2008). *Offshore Hydromechanics*. Delft University of Technology.

Lamb, H. (1932). *Hydrodynamics*. University of Michigan.

Wehausen, J.V., and Laitone E.V. (2002). *Surface Waves Online*. Regents of the University of California.

Holthuijsen, L.H., (2007). *Waves in oceanic and coastal waters.* Cambridge University Press.

Fan, M., Li, D., Liu, T., Ran, A., and Ye, W. (2010). An innovative synthetic mooring solution for an octagonal FPSO in shallow waters. In *proceedings of the ASME 2010*

29th International Conference on Ocean, Offshore and Arctic Engineering, Shanghai.

Bandas, J., and Falzarano, J.M. (2011). A Numerical Investigation into the Linear Seakeeping Ability of the T-Craft. In *proceedings of the 11th International Conference on Fast Sea Transportation FAST 2011, Hawaii.*

Durran, D.R. (2015). *Encyclopedia of Atmospheric Sciences*. University of Washington.

Hong, S.Y., Kim, J.H., Cho, S.K., Choi, Y.S., and Kim, Y.S. (2005). Numerical and experimental study on hydrodynamic interaction of side-by-side moored multiple vessels. *Ocean Engineering* 32(1), 783–801.

Chen, G.R., and Fang, M.C. (2001).Hydrodynamic interactions between two ships advancing in waves. *Ocean Engineering* 28(1), 1053-1078.

Putranto, T. (2018). The Longitudinal Strength Analysis of Aquaculture Floating Structure in Indonesia Sea Water. *International Journal of Mechanical and Production Engineering Research and Development* 8(2), 283-290.

Kim, M.S., Ha, M.K., and Kim, B.W. (2003). Relative Motions between LNG-FPSO and Side-by-Side positioned LNG Carrier in Waves. In *proceedings of the Thirteenth International Offshore and Polar Engineering Conference, Hawaii.*

Wu, X.J., and Price, W.G. (1987). Hydrodynamic interactions between two ships advancing in waves. *Ocean Engineering* 9(2), 58-66.

Smith, D.J. (1996). Simplified First Order Motion Analysis of a Moored FPSO. *Journal of the Society for Underwater Technology* 22(1), 3-13.

Xu, X., Li, X., Yang J.M., and Xiao, L.F. (2016). Hydrodynamic Interactions of Three Barges in Close Proximity in a Floatover Installation. *China Ocean Engineering* 30(3), 343-358.

Jin, J.Z., Magee, A.R., Han M.M., Hoff J.R., Hermundstad, E.M., Hellan, Ø., Wang, C.M., (2017). Internal fluid effect inside a floating structure: from frequency domain solution to time domain solution. In *proceedings of the ASME 2017 36th International Conference on Ocean, Offshore and Arctic Engineering, Trondheim.*

Appendix A

Laplace equation and Bernoulli equation

In potential theory, the velocity component in any chosen direction is the derivative of this potential function in any chosen direction:

$$\dot{x} = \frac{\partial \Phi}{\partial x} \quad \dot{y} = \frac{\partial \Phi}{\partial y} \quad \dot{z} = \frac{\partial \Phi}{\partial z} \tag{A. 1}$$

All potential theory solutions must satisfy the rotation free condition and the Laplace equation. The former describes the irrationality of the island in the ideal flow that can be written for (x,y)-plane as:

$$\begin{aligned} \dot{x} &= \frac{\partial \Phi}{\partial x} \qquad \text{so:} \quad \frac{\partial \dot{x}}{\partial y} = \frac{\partial}{\partial y}\left(\frac{\partial \Phi}{\partial x}\right) = \frac{\partial^2 \Phi}{\partial y \partial x} \\ \dot{y} &= \frac{\partial \Phi}{\partial y} \qquad \text{so:} \quad \frac{\partial \dot{y}}{\partial x} = \frac{\partial}{\partial x}\left(\frac{\partial \Phi}{\partial y}\right) = \frac{\partial^2 \Phi}{\partial x \partial y} \end{aligned} \tag{A. 2}$$

Obviously,

$$\frac{\partial^2 \Phi}{\partial y \partial x} = \frac{\partial^2 \Phi}{\partial x \partial y} \qquad \text{one can write:} \quad \frac{\partial \dot{x}}{\partial y} - \frac{\partial \dot{y}}{\partial x} = 0 \tag{A. 3}$$

This can be applied to other planes likewise:

$$\frac{\partial \dot{x}}{\partial y} - \frac{\partial \dot{y}}{\partial x} = 0 \qquad \frac{\partial \dot{x}}{\partial z} - \frac{\partial \dot{z}}{\partial x} = 0 \qquad \frac{\partial \dot{z}}{\partial y} - \frac{\partial \dot{y}}{\partial z} = 0 \tag{A. 4}$$

The latter, Laplace equation, as well as the Bernoulli equation, are two essential functions to solve the potential function. In this chapter, they have been derived by mass balance and momentum balance governing equations separately for incompressible flow.

At first, a balance equation for an arbitrary property μ as the governing equation can be represented as an expression of the storage of μ during time interval Δt, the net import of μ during Δt, and the local production of μ during Δt as:

$$\text{Storage}_{\mu\ in\ \Delta t} = NetImport_{\mu\ in\ \Delta t} + Prodcution_{\mu\ in\ \Delta t} \tag{A. 5}$$

The first term in the equation A.5, $\text{Storage}_{\mu\ in\ \Delta t}$, can be expressed as:

$$\text{Storage}_{\mu\ in\ \Delta t} = quantity\ at\ (t + \Delta t) - quantity\ at\ (t) = \frac{\partial \mu}{\partial t} \Delta x \Delta y \Delta z \Delta t \tag{A. 6}$$

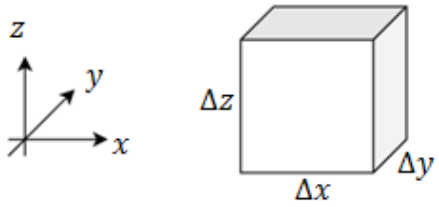

Figure A.1: Storage of μ during time interval Δt

The second term in the equation A.5, $NetImport_{\mu\ in\ \Delta t}$, can be expressed as:

$$NetImport_{\mu\ in\ \Delta t} = import - export$$

$$= -\frac{\partial \mu u_x}{\partial x}\Delta x\Delta y\Delta z\Delta t - \frac{\partial \mu u_y}{\partial y}\Delta x\Delta y\Delta z\Delta t - \frac{\partial \mu u_z}{\partial z}\Delta x\Delta y\Delta z\Delta \quad (A.7)$$

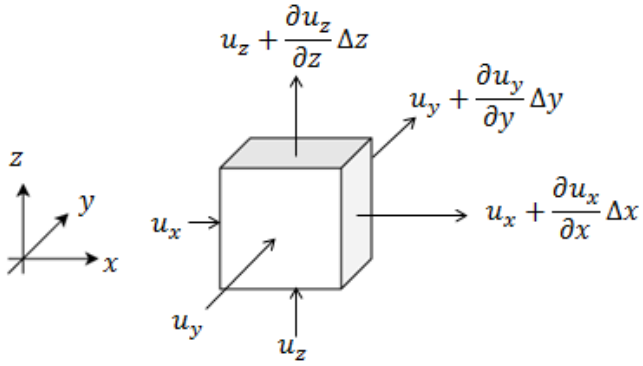

Figure A.2: Net import in the x-, y- and z-directions during Δt

The last term in the equation A.5, $\text{Storage}_{\mu\ in\ \Delta t}$, can be expressed as:

$$Prodcution_{\mu\ in\ \Delta t} = S\Delta t\Delta x\Delta y\Delta z \quad (A.8)$$

In which S is the production of μ per unit time, per unit volume.

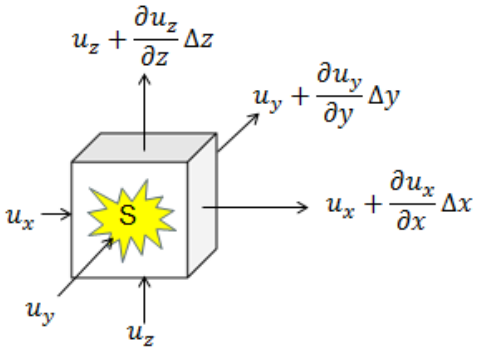

Figure A.3: local production of μ during Δt

Combining equations A.4 through A.7 and eliminating the same term $\Delta x\Delta y\Delta z\Delta t$, the product of the volume and time interval, to obtain:

$$\frac{\partial \mu}{\partial t} + \frac{\partial \mu u_x}{\partial x} + \frac{\partial \mu u_y}{\partial y} + \frac{\partial \mu u_z}{\partial z} = S \quad (A.9)$$

In which $\frac{\partial \mu}{\partial t}$ is so called the local rate of change of μ, $\frac{\partial \mu u_x}{\partial x} + \frac{\partial \mu u_y}{\partial y} + \frac{\partial \mu u_z}{\partial z}$ are advective terms and S is the source term.

The arbitrary property μ equals density ρ that is assumed as a constant in the beginning if one considers the mass balance so that it can get rid of the time and space derivatives. Besides, there is no production of water in this case, so the source is zero. Removing the density in equation A.9 provides the **continuity equation** A.10, which is a partial differential equation describing the transport behavior of conserved quantities for incompressible flow.

$$\frac{\partial u_x}{\partial x}+\frac{\partial u_y}{\partial y}+\frac{\partial u_z}{\partial z}=0 \qquad (A.10)$$

Utilizing the continuity equation A.10 to the velocities in the equation A.1 supplies the **Laplace equation** for an incompressible fluid as:

$$\frac{\partial^2 \Phi}{\partial x^2}+\frac{\partial^2 \Phi}{\partial y^2}+\frac{\partial^2 \Phi}{\partial z^2}=0 \qquad (A.11)$$

Similarly, replace μ by momentum density $\rho\vec{u}$ to obtain the momentum balance equations as follows:

$$\begin{aligned}
&\frac{\partial(\rho u_x)}{\partial t}+\frac{\partial u_x(\rho u_x)}{\partial x}+\frac{\partial u_y(\rho u_x)}{\partial y}+\frac{\partial u_z(\rho u_x)}{\partial z}=S_x\\
&\frac{\partial(\rho u_y)}{\partial t}+\frac{\partial u_x(\rho u_y)}{\partial x}+\frac{\partial u_y(\rho u_y)}{\partial y}+\frac{\partial u_z(\rho u_y)}{\partial z}=S_y\\
&\frac{\partial(\rho u_z)}{\partial t}+\frac{\partial u_x(\rho u_z)}{\partial x}+\frac{\partial u_y(\rho u_z)}{\partial y}+\frac{\partial u_z(\rho u_z)}{\partial z}=S_z
\end{aligned} \qquad (A.12)$$

In the momentum balance, the production of momentum S equals to the sum of forces comes from Newton's law. Thus, for the momentum balance in the x-direction:

$$\frac{\partial u_x}{\partial t}+u_x\frac{\partial u_x}{\partial x}+u_y\frac{\partial u_x}{\partial y}+u_z\frac{\partial u_x}{\partial z}=-\frac{1}{\rho}\cdot\frac{\partial p}{\partial x}=-\frac{\partial}{\partial x}\left(\frac{p}{\rho}+gz\right) \qquad (A.13)$$

Applying the rotational free condition in equation A.4:

$$\begin{aligned}
&\frac{\partial u_x}{\partial t}+\frac{1}{2}\frac{\partial}{\partial x}({u_x}^2+{u_y}^2+{u_z}^2)=-\frac{\partial}{\partial x}(\frac{p}{\rho}+gz)\\
&\frac{\partial}{\partial x}\left[\frac{\partial \Phi}{\partial t}+\frac{1}{2}\left({u_x}^2+{u_y}^2+{u_z}^2\right)+\frac{p}{\rho}+gz\right]=0
\end{aligned} \qquad (A.14)$$

Hence, an equation that states an increase in the speed of a fluid arises concurrently with a decrease in pressure or a decrease in the potential energy of the fluid is obtained, which is as known as the **Bernoulli equation** as follows:

$$\frac{\partial \Phi}{\partial t}+\frac{1}{2}\left({u_x}^2+{u_y}^2+{u_z}^2\right)+\frac{p}{\rho}+gz=0 \qquad (A.15)$$

Appendix B

Added mass

The added masses due to the hydrodynamic interactions between the two islands are shown as follows:

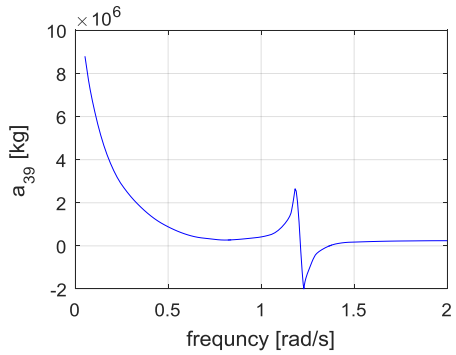

(a) a_{39}

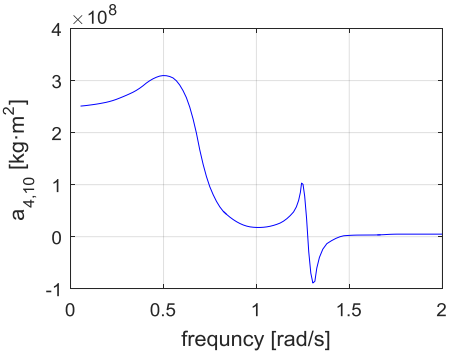

(b) $a_{4,10}$

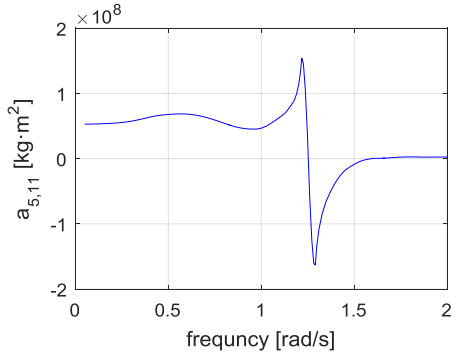

(c) $a_{5,11}$

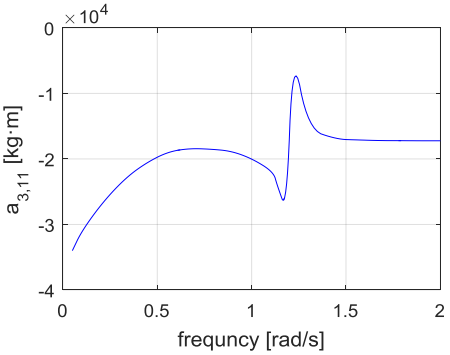

(d) $a_{3,11}$

Appendix C

Damping coefficients

The damping coefficients due to the hydrodynamic interactions between the two islands are shown as follows:

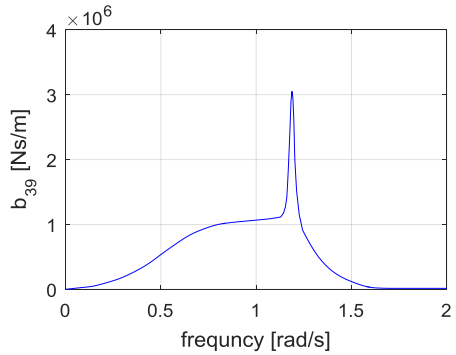

(a) b_{39}

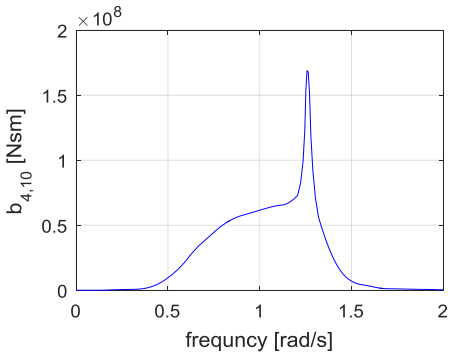

(b) $b_{4,10}$

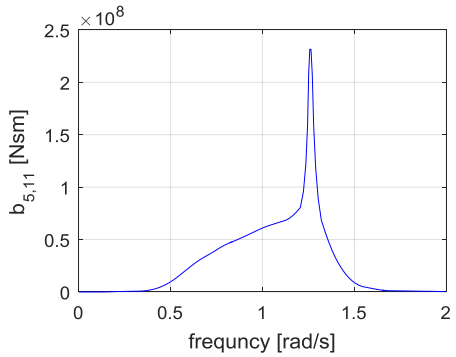

(c) $b_{5,11}$

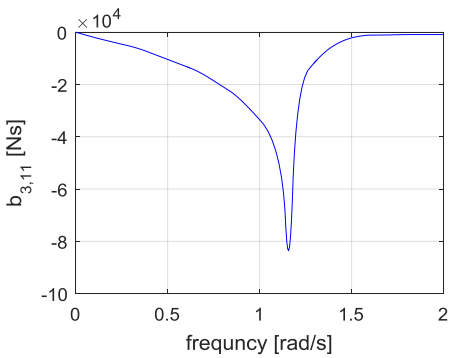

(d) $b_{3.11}$